Coupled Interannual Rossby Waves in a Quasigeostrophic Ocean–Atmosphere Model

RICCARDO FARNETI

National Oceanography Centre, Southampton, Southampton, United Kingdom

(Manuscript received 20 December 2005, in final form 7 April 2006)

ABSTRACT

Rossby wave propagation is investigated in the framework of an idealized middle-latitude quasigeostrophic coupled ocean–atmosphere model. The Rossby waves are observed to propagate faster than both the classical linear theory (unperturbed solution) and the phase speed estimates when the effect of the zonal mean flow is added (perturbed solution). Moreover, using statistical eigentechniques, a clear coupled Rossby wave mode is identified between a baroclinic oceanic Rossby wave and an equivalent barotropic atmospheric wave. The spatial phase relationship of the coupled wave is similar to the one predicted by Goodman and Marshall, suggesting a positive ocean–atmosphere feedback. It is argued that oceanic Rossby waves can be efficiently coupled to the overlying atmosphere and that the atmospheric coupling is capable of adding an extra speedup to the wave; in fact, when the ocean is simply forced, the Rossby wave propagation speed approaches the perturbed solution.

1. Introduction

In recent years there has been a growing interest in the scientific community in studying ocean–atmosphere coupled models (Liu 1993; Frankignoul et al. 1997; Barsugli and Battisti 1998; Goodman and Marshall 1999, hereinafter GM99; Ferreira et al. 2001; White et al. 1998; Neelin and Weng 1999; White 2000a; Gallego and Cessi 2000; Cessi and Paparella 2001; Colin de Verdière and Blanc 2001; Kravtsov and Robertson 2002, to mention a few). Different approaches have been used and different results, sometimes in disagreement, have been found. Nevertheless, there are a few key findings that can be pointed out. There is some evidence that the ocean can interact through feedback mechanisms (e.g., Latif and Barnett 1994, 1996; Barsugli and Battisti 1998; Pierce et al. 2001; Hogg et al. 2006; Kravtsov et al. 2006), and it has also been suggested that oceanic Rossby waves play a major role in the coupling physics (e.g., Jin 1997; GM99; Ferreira et al. 2001; Kravtsov and Robertson 2002; Arzel and Huck 2003). These studies on atmosphere–ocean coupling could also help understand the differences between theoretical and observed Rossby wave phase speeds (Frankignoul et al. 1997; Ferreira et al. 2001; White et al. 1998), although different answers are usually argued.

For instance, Frankignoul et al. (1997) studied the decadal variability of the extratropical ocean forced by stochastic winds. They found a baroclinic response consisting of a Rossby wave traveling at twice the theoretical speed, and concluded that this could be a reason for the fast speeds observed by Chelton and Schlax (1996). The model of Frankignoul et al. (1997) was simple, with a flat-bottomed two-layer ocean with neither a western boundary nor a mean flow, the latter of which has been proved to be of great importance in Rossby wave propagation (Killworth et al. 1997). Although there is a lack of reality in these models, simple models are often able to predict the basic coupling mechanisms (Barsugli and Battisti 1998), and it seems very probable that, even if neither the mechanisms nor the magnitude are completely understood, coupling effects are able to modify Rossby wave phase speeds.

Two of the theoretical studies that are the most complete to date are given by GM99 and Ferreira et al. (2001). GM99 used a quasigeostrophic (QG) atmosphere overlying a QG ocean where the coupling mechanisms were both wind stress and thermal forcing. In their analytical model they found that coupled modes in which baroclinic Rossby waves can grow (unstable modes) exist under some circumstances through the linear interaction between traveling oceanic Rossby

Corresponding author address: Dr. Riccardo Farneti, GFDL/AOS Program, Princeton University, Princeton, NJ 08542.
E-mail: riccardo.farneti@noaa.gov

DOI: 10.1175/JPO3061.1

waves and forced stationary atmospheric planetary waves. The response in the atmosphere to the thermal forcing is equivalent barotropic, and the resulting behavior need not be a first baroclinic mode. Furthermore, GM99 pointed out that the atmosphere and the ocean need not be in phase (high pressures located above warm water) for the growing mode to exist, but that for the case of the Antarctic Circumpolar Wave growing modes occur if surface air pressure is in phase with sea surface temperature (SST), contrary to the observations in White and Peterson (1996). A similar result was also found by van der Avoird et al. (2002) who, using a linear stability analysis of a two-layer coupled model, described a coupled mode of the interdecadal period originating from the interaction between a baroclinic Rossby wave and a quasi-stationary atmospheric equilibrated planetary wave with the same mechanisms as that in the advective case of GM99.

Extending the work by GM99, Ferreira et al. (2001) found similar patterns. Within an equivalent barotropic atmospheric response leading to coupled growing modes, Ferreira et al. (2001) show that positive feedback can occur both with quadrature between SST and sea level pressure (SLP) when temperature anomalies are modulated by advection, and with a "nearly in phase" response if entrainment dominates. As in Frankignoul et al. (1997), the phase speed of the baroclinic Rossby wave was observed to increase because of larger wavelengths resulting from the coupling, leading to increased phase speeds.

A different mechanism is brought forward in Colin de Verdière and Blanc (2001), in which the authors propose a thermal rather than mechanical process to explain the feedback resulting in the SST–SLP phase relationship. The simple ocean used in all of these studies could be a weakness of the results but the atmosphere is more likely to be the cause of any misrepresentation.

GM99's theory has not been highlighted in satellite observations so far. These are used by White et al. (1998) to study the interaction between the atmosphere and ocean, and analytical models are developed to be used in synergy with these studies. White et al. (1998) analyzed anomalies in the sea level height (SLH), SST, and meridional surface winds (MSW) signatures in the Pacific Ocean. They found a 90° shift between SST and SLH in an advection mechanism as well as faster Rossby wave phase speeds in the midlatitudes and slower speeds in the subtropics, reducing the characteristic β refraction of Rossby waves. The authors argued that the effect of coupling was due to the introduction of a supplementary zonal phase speed component that increases the theoretical phase speed resulting from a SST-induced meridional anomalous heat transport by Ekman velocities. Moreover, analyzing data from the Indian Ocean, White (2000a) observed slower speeds and argued that in the Indian Ocean the phase relation between SST and MSW was opposite that in the Pacific, allowing for an eastward phase speed resulting in slower Rossby wave propagation. Based on Ocean Topography Experiment (TOPEX)/Poseidon (T/P) observations in both White et al. (1998) and White (2000a) different analytical models and theories for the two oceans are derived.

However, the GM99 ocean–atmosphere phase relationship, involving an equivalent barotropic atmosphere with high (low) SLP anomalies associated with warm (cold) SST anomalies, has been previously theorized (Frankignoul 1985; Shutts 1987; Marshall and So 1990; Ferreira et al. 2001), modeled (Kushnir and Held 1996; Frankignoul et al. 2000; van der Avoird et al. 2002), and observed (Deser and Blackmon 1993; Kushnir 1994; Latif and Barnett 1996) for interannual-to-decadal periods. We will show how this mechanism, without the many assumptions and simplifications applied to the GM99 theoretical work, naturally arises in our model.

Although a general coupled Rossby wave model, describing the interaction of the oceanic Rossby wave with the overlying atmosphere, on which the scientific community has yet agreed, the literature presented here gives clear examples of the increasing interest and efforts on the study of coupled mechanisms in which oceanic Rossby waves are modified either in their structures or in their phase speeds.

The main goals of the study presented in this paper are the identification of the atmospheric influence and possible positive feedback on the oceanic Rossby wave propagation. We will focus on the possibility of a positive coupling between the oceanic wave and the atmosphere at middle latitudes, trying to identify a coupled wave mode in a fully nonlinear fully coupled ocean–atmosphere model and its subsequent response in the wave propagation. The GM99's mechanical process is found, among others, to be the strongest and the most influential. Comparisons with previous theories and observations will follow.

In section 2 we briefly describe the model employed, in section 3 we identify the Rossby wave activities in the model, and we characterize their main properties with the help of statistical analyses in section 4. We then proceed to isolate a coupled Rossby wave explaining the relationships with the atmospheric variables in section 5, and we conclude with a discussion of the results in section 6.

2. Model description

We use the Quasigeostrophic Coupled Model (Q-GCM) (Hogg et al. 2003a,b). The model is symmetric around the ocean–atmosphere interface, and the mixed layer is embedded in the first layer for both the atmosphere and ocean.

For a flat-bottomed three-layer configuration, the QG potential vorticity (QGPV) equation is

$$\partial_t q_i + J(\psi_i, q_i) = f_0 \mathbf{Ae} + A_2 \nabla^4 \psi_i - A_4 \nabla^6 \psi_i, \quad (1)$$

where q_i and ψ_i are the layer potential vorticities and streamfunctions respectively, $J(a, b) = a_x b_y - a_y b_x$ is the Jacobian, f_0 is the Coriolis parameter at the central latitude of the domain in the frozen β plane ($f = f_0 + \beta_y$), and subscripts denote derivatives. The vectors on the right, **A** and **e**, are the matrices containing the forcing terms and the ocean and atmosphere entrainment vectors, respectively. The last two terms on the right-hand side of (1) correspond to Laplacian diffusion and biharmonic viscosity, respectively.

The system interacts via the two mixed layers, where stress and fluxes are parameterized and then entrained into their respective first layer. The mixed layer temperature equations are expressed as

$$\partial_t T + \boldsymbol{\nabla} \cdot (\mathbf{u}T) = \frac{T}{H_m} \begin{Bmatrix} w_{\text{oek}} \\ -w_{\text{aek}} \end{Bmatrix} + K_2 \nabla^2 T - K_4 \nabla^4 T + \frac{1}{H_m} \begin{Bmatrix} -\dfrac{F_{\text{o0}} - F_{\text{om}}}{\rho_o C_{\text{po}}} \\ \dfrac{F_{\text{a0}} - F_{\text{om}}}{\rho_a C_{\text{pa}}} \end{Bmatrix}, \quad (2)$$

where ρ_o and ρ_a are the ocean and atmosphere density, w_{oek} and w_{aek} are their Ekman pumping, C_{po} and C_{pa} are their specific heat capacity, H_m is their mixed layer thickness, and **u** are the mixed layer velocities. Only the atmospheric mixed layer has a variable height resulting from numerical necessity, whereas the depth of the oceanic mixed layer is fixed.

The second and third terms on the right-hand side of (2) are Laplacian and biharmonic diffusions. The last term in (2) represents the fluxes at the top (F_m) and surface (F_0) of the mixed layer.

For every experiment the Q-GCM is initially run for 20 yr, during which time the ocean spins up and reaches a steady state. Then, the run is continued for a total of 200 model years. For more details and a clear derivation of the model equations, we refer to Hogg et al. (2003a,b).

Experimental design and basic-state solutions

The oceanic and atmospheric parameters used in the standard three-layer basin ocean configuration are listed in Table 1. We opted for a relatively coarse resolution in the ocean ($\Delta x = 40$ km), because we aim to identify large-scale coupled ocean–atmosphere interactions.

TABLE 1. List of the standard oceanic and atmospheric parameters of the Q-GCM used in this study.

Parameters	Value	Description
	Ocean	
Z_i	3	No. of layers
Δx	40 km	Horizontal grid spacing
(X, Y)	(11 520, 4800) km	Domain size
H_i	(300, 1100, 2600) m	Mean layer thicknesses
H_m	100 m	Mixed layer thickness
g_i'	(0.05, 0.025) m s^{-2}	Reduced gravities
ρ_o	1×10^3 kg m^{-3}	Density
C_{po}	4×10^3 J (kg K)$^{-1}$	Specific heat capacity
K_2	5.7×10^2 m^2 s^{-1}	∇^2 diffusion coefficient
K_4	8×10^{10} m^4 s^{-1}	∇^4 diffusion coefficient
A_4	4×10^{10} m^4 s^{-1}	∇^4 viscosity coefficient
f_0	7.292×10^{-5} s^{-1}	Coriolis parameter, $\phi = 30°$
β	1.982×10^{-11} (m s)$^{-1}$	df/dy (30°)
a_i	(53.1, 35.6) km	Rossby radii (30°)
f_0	9.374×10^{-5} s^{-1}	Coriolis parameter, $\phi = 40°$
β	1.753×10^{-11} (m s)$^{-1}$	df/dy (40°)
a_i	(41.3, 27.9) km	Rossby radii (40°)
	Atmosphere	
Z_i	3	No. of layers
Δx	120 km	Horizontal grid spacing
(X, Y)	(15 360, 7680) km	Domain size
H_i	(2000, 3000, 4000) m	Mean layer thicknesses
H_m	100 m	Minimum mixed layer thickness
g_i'	(1.2, 0.4) m s^{-2}	Reduced gravities
ρ_a	1 kg m^{-3}	Density
C_{pa}	1×10^3 J (kg K)$^{-1}$	Specific heat capacity
K_2	2.7×10^4 m^2 s^{-1}	∇^2 diffusion coefficient
K_4	3×10^{14} m^4 s^{-1}	∇^4 diffusion coefficient
A_4	2×10^{14} m^4 s^{-1}	∇^4, viscosity coefficient
Λ	35 W m^{-2} K^{-1}	Sensible and latent heat flux coefficient

We explore the response of the model at two different central latitudes, corresponding to 30° and 40°; for the two cases, our model barely resolves the first Rossby radius of deformation, but not the second one. The basin dimensions are fairly large and, in particular, the ocean is very wide in order to study the zonal propagation of planetary waves under the effect of atmospheric coupling. This has the advantage of using a quasi-channel configuration but retaining the effects of meridional boundaries. In fact, Rossby waves are dissipated at the western boundary and any coupled Rossby mode will be affected by this interaction (Goodman and Marshall 2003). Viscosities are set to

their minimum value, ensuring that stability and no-slip boundary conditions are enforced.

The averaged ocean forcing fields $\tau = (\tau^x, \tau^y)$ and relative Ekman pumping w_{oek} are shown in Fig. 1, together with the oceanic SST. The flow responds to the wind stress with a double-gyre solution, a subpolar and a subtropical gyre, and the presence of a strong boundary current, separating at the center of the meridional extension of the basin, which will play a major role in damping the incident planetary waves in the model.

3. Detection and identification of Rossby waves

The Q-GCM is run for 200 model years at two central latitudes of $\phi = 30°$ and 40° for the parameters listed in Table 1. Oceanic and atmospheric variables are saved every 10 days in order to have a dense temporal sampling, which is useful for the statistical techniques applied later on in the study and enabling direct comparisons with satellite measurements such as TOPEX/Poseidon, which provides observations approximately every 10 days.

We are then ready to identify the propagation of the oceanic Rossby waves generated by the unsteady winds in the model (Fig. 1) and their basic properties. We begin by plotting Hovmöller diagrams (time–longitude plots at a given meridional position in the ocean basin domain) of the second interface height (OCH2), corresponding to thermocline displacements. The Hovmöller diagrams shown are for the north subtropical gyre, for correspondence with the real oceans at these latitudes; nevertheless, they show similar patterns at different locations.

Because we are interested in westward-propagating waves, we apply a westward filter to the data (Cipollini et al. 2000), the results of which are shown in Fig. 2 for a particular time interval. Here, clear signals of crests and troughs are visible with a strong zonal variation in both amplitude and propagating speed. For comparison purposes, we also plotted the results from a previous run, with the same characteristics, at $\phi = 20°$. By following crests we can estimate an approximate velocity of the dominant signals, and a simple inspection of the diagrams reveals the theoretical increase in phase speed as we move toward lower latitudes. With this crude estimation, at $\phi = 30°$ the phase speed is around 6.5 cm s^{-1} and at $\phi = 40°$ around 5 cm s^{-1}. These are relatively high phase speeds because in the simulations our Rossby radii give us velocities of 5.2 and 2.9 cm s^{-1} at 30° and 40°, respectively, for the first baroclinic Rossby wave mode.

The high phase speeds identified seem to agree with some observations, for instance, Osychny and Cornillon (2004), who find differences in wave propagation stronger at higher latitudes. Hovmöller plots of SST anomalies reveal similar results for all central latitudes.

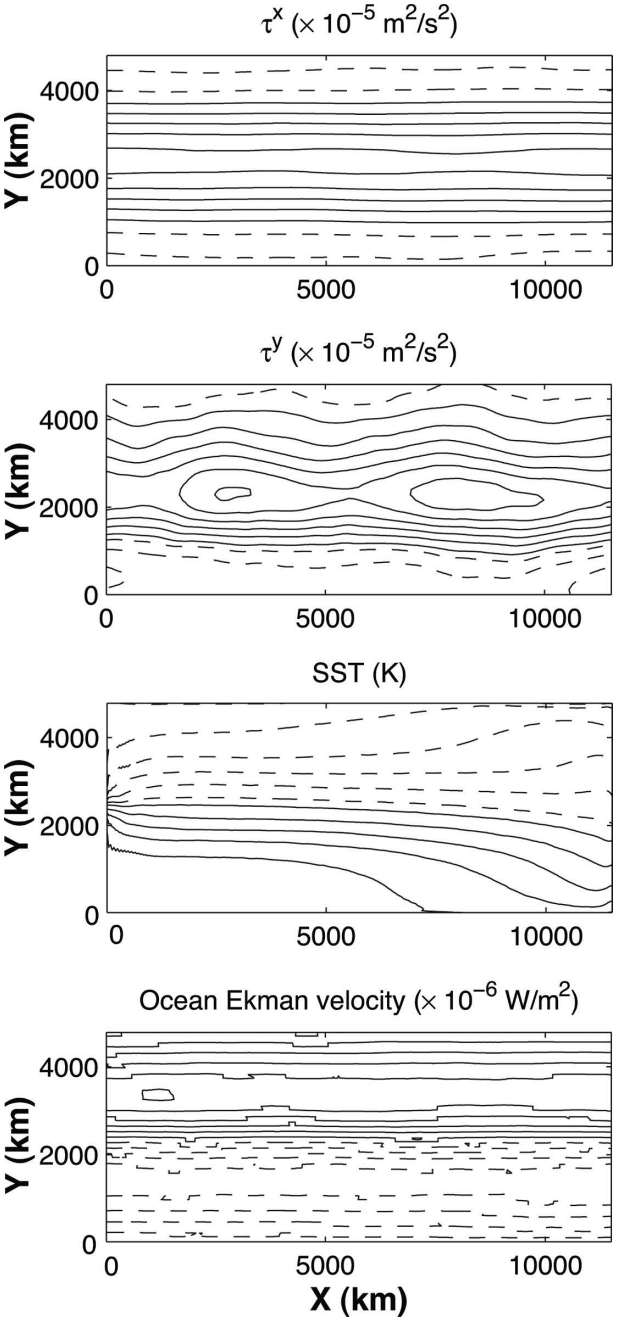

FIG. 1. (top to bottom) Average of τ^x [contour interval (CI) = 20], τ^y (CI = 3), SST (CI = 3), and w_{oek} (CI = 0.2). Negative values are represented by dashed lines.

Another fundamental feature in Fig. 2 is the apparent breaking and instability of the waves, which is stronger as we move away from the equator. However, the effects of and on the instabilities will be the subject of a forthcoming paper.

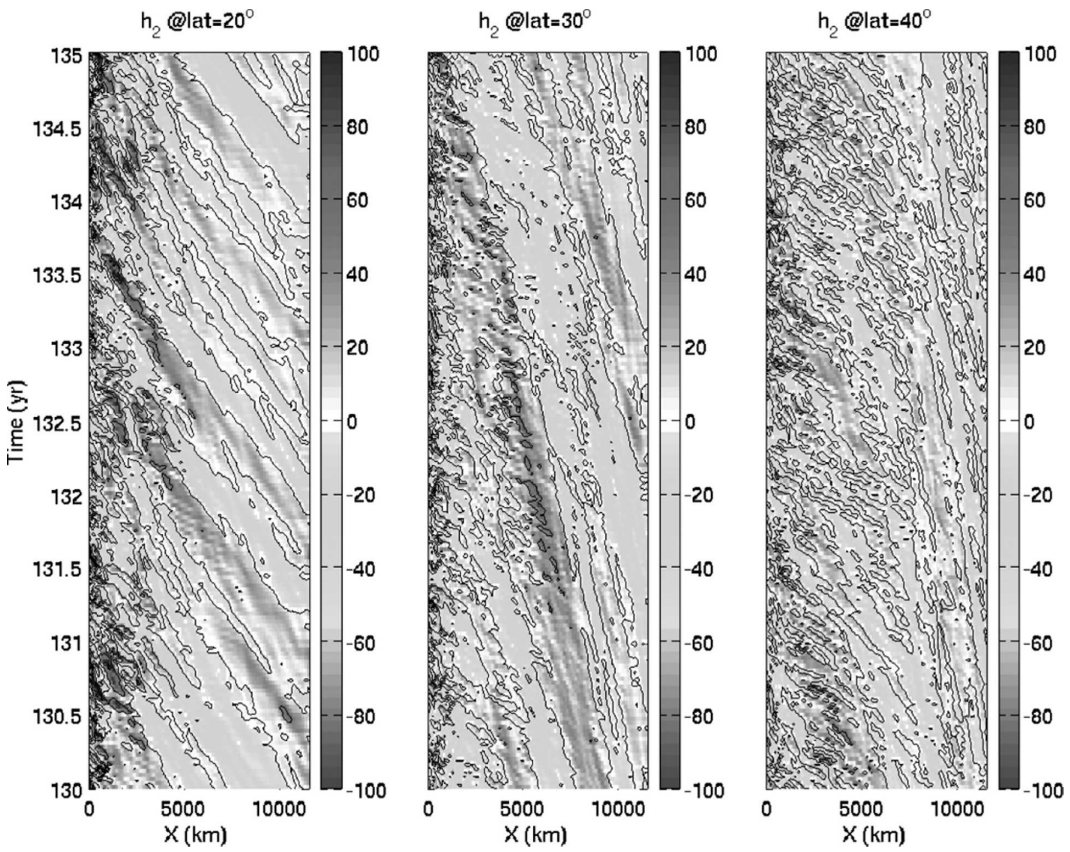

FIG. 2. Hovmöller plots of the westward-filtered second interface height OCH2 (m), representative of the thermocline displacements, for three different central latitudes: ϕ = (left) 20°, (middle) 30°, and (right) 40°.

A complementary and more accurate identification of the spectral characteristics of the identified Rossby waves is achieved through a fast Fourier transform (FFT) of the westward-filtered data, resulting in frequency–wavenumber spectra. To this purpose we applied a temporal bandpass filter to the data between 1 and 5 yr at every spatial location in order to suppress the high frequencies and the decadal–interdecadal signals.

The FFT analysis plotted in Fig. 3 reveals Rossby waves that are propagating much faster than the unperturbed (dashed lines) and the perturbed dispersion relation (solid lines) predict, with mean peaks showing phase speeds around 2 times the unperturbed values at both central latitudes. Here, we will refer to "perturbed solution" to the dispersion relation computed with the inclusion of a zonal mean flow while the "unperturbed solution" corresponds to the classical linear dispersion relation (For the computation of perturbed solutions see the appendix). Both Hovmöller and perturbed solutions are computed at the northern part of the subtropical gyre, corresponding to the latitudes tested here. In our three-layer system we found only small variations in the dispersion relation when including the model zonal mean flows. Following the theory of de Szoeke and Chelton (1999), and making use of our density jumps and mean layer depths, we should reach a speedup of about 1.4. However, in the calculations given in the appendix, the maximum speedup was found to be of around 1.22, and this corresponds to the solid lines in Fig. 3.

For the case at $\phi = 30°$ (left panel of Fig. 3) we find wave speeds ranging from 6 to 9 cm s^{-1}, all of which are much higher than the unperturbed and perturbed theory would predict. The main peak in the spectra has a period P of about 2.5 yr. We can see that spectral peaks fall into the long nondispersive range, where the phase speed is well approximated by $c_x = -\beta a^2$, where a is the Rossby radius of deformation, and tends to diverge from the linear dispersion relation as the wavelength decreases, consistently with Wunsch and Zang (1999), Osychny and Cornillon (2004), and Killworth and Blundell (2005).

For the central latitude $\phi = 40°$ (right panel of Fig. 3) the results are qualitatively very similar. The main peak is around P = 3–3.5 yr with phase speeds of about 4–4.5

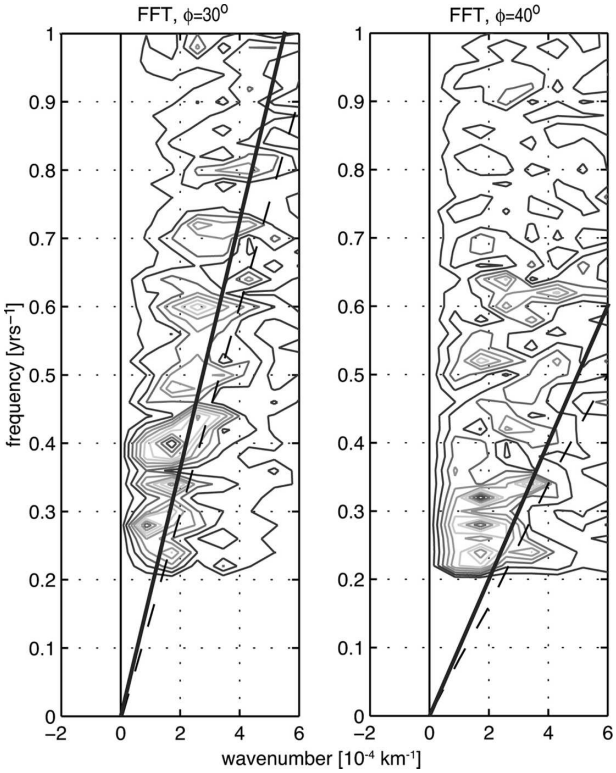

FIG. 3. Frequency–wavenumber spectra of OCH2 anomalies at (left) $\phi = 30°$ and (right) $\phi = 40°$. Magnitude is normalized by its maximum value for each case, with increasing magnitude toward lighter shadings. The broken line represents the theoretical dispersion relation at the two central latitudes computed from the theoretical dispersion relation with the model's Rossby radii. The solid lines are the computed perturbed dispersion relation with the inclusion of a zonal mean flow (see the appendix). The mean flow speedup is about 1.2 for typical examples, close to the suggested value of 1.4 by de Szoeke and Chelton (1999).

cm s^{-1}. The wavenumber of the main peaks is around 2×10^{-7} m^{-1}, which corresponds to a wavelength $\lambda = 5 \times 10^6$ m. Although quite a long wave, GM99 found in their analytical results $k = \pi\,(5500\text{ km})^{-1} = 5.7 \times 10^{-7}$ or $\lambda \sim 1 \times 10^7$ m as the wavelength of maximum growth at a decadal period ($\omega = 2 \times 10^{-8}\ s^{-1}$) for their coupled Rossby mode. Our wavelengths are different because of the choice in our basin dimensions and, if an atmospheric coupling is occurring, an increase in the wavelengths of the coupled waves is expected, as suggested by Ferreira et al. (2001).

Generally, we discovered very fast Rossby waves in our model runs, all with phase speeds faster than predicted by the linear theory, with increasing differences as we move toward higher latitudes (Chelton and Schlax 1996; Killworth et al. 1997). Although some peaks in the FFT analyses fall into either the unperturbed or the perturbed dispersion relation, one or two major peaks at both central latitudes are clearly too fast and are not explained by the inclusion of a sheared mean zonal flow; this result makes us think of the possibility of a positive coupling with the atmosphere, responsible for an additional speedup of the wave. Coupled Rossby modes have been identified in data (White et al. 1998; White 2000a, 2001) and simple analytical–numerical models (GM99; Goodman and Marshall 2003), but whether they really exist in fully coupled models of intermediate complexity is still unclear and the processes involved within a full dynamics model are not completely understood.

4. Principal component analysis of the oceanic and atmospheric variability

The ocean circulation in the model is dominated by a double-gyre circulation (subtropical and subpolar) separated by a narrow and strong zonal current, where the SST presents a sharp front. The channel atmosphere is instead characterized by a zonally symmetric circulation, with sloping interface heights (ATH1 and ATH2) toward the south resulting from the radiation condition of heating in the southern region and cooling in the north.

The atmospheric dynamics are then inferred from an empirical orthogonal function (EOF) analysis (Preisendorfer and Mobley 1988). The first four EOFs of the two unfiltered interface heights, ATH1 and ATH2, explain around 37% and 21%, respectively, of the total variance (not shown). EOF-1 has a wavenumber-3 structure, apparently propagating eastward, in quadrature with EOF-2 of similar eigenvalue, and a standing annular wavenumber-3 mode is dominating the third EOF. Similar results are found when applying the principal component analysis to the unfiltered atmospheric surface temperature (AST). In fact, for both central latitudes, a wavenumber-3 propagating wave and the standing annular wavenumber-3 mode explain most of the variance.

The results obtained with the EOFs analysis of the unfiltered data are in agreement with previous similar studies (Kravtsov et al. 2003, 2006; Hogg et al. 2006); however, they do not shed much light on the atmospheric wave propagation and we need a more powerful technique to address the question of what are the characteristics of the wave dynamics in both ocean and atmosphere and whether they are related. To this end, we will next apply a variation of EOFs to our data, the complex empirical orthogonal function (CEOF) analysis, more suitable for studying propagating waves.

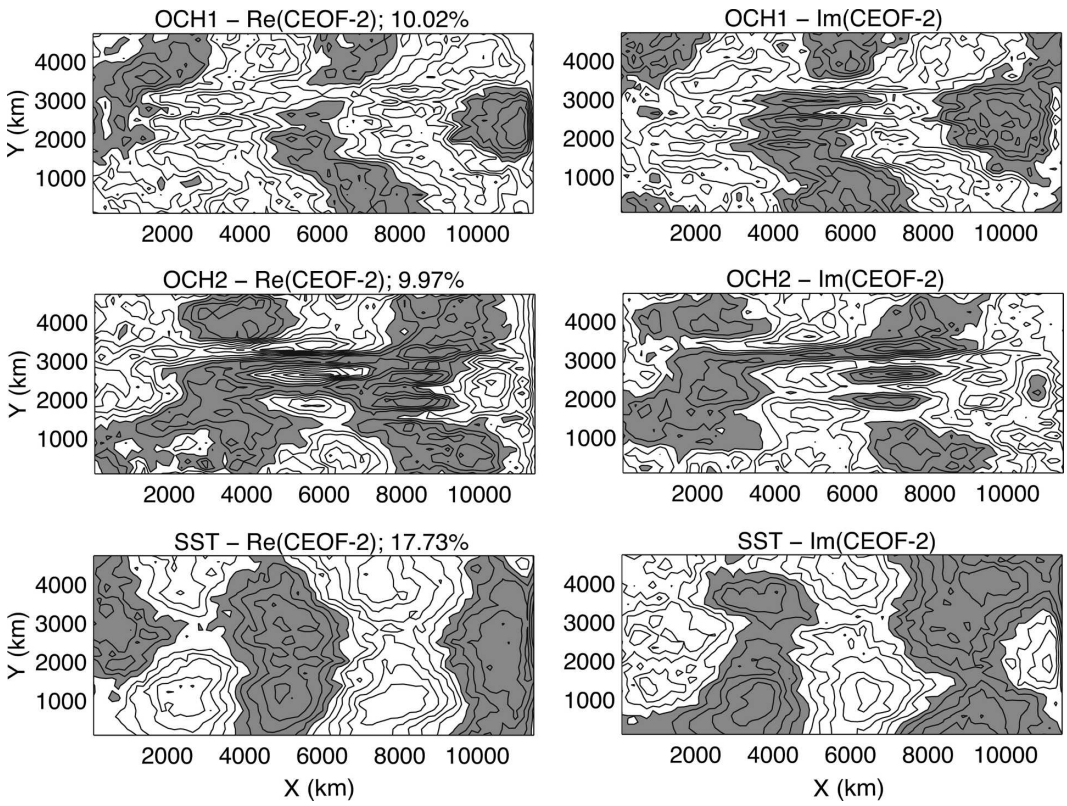

FIG. 4. (left) The real and (right) imaginary spatial patterns of the second CEOF modes of the filtered (top) OCH1, (middle) OCH2, and (bottom) SST at $\phi = 40°$. Respectively, 10.02%, 9.97%, and 17.73% of the variance is explained. Negative weights are shaded.

Patterns of observed Rossby waves in both ocean and atmosphere

Statistical eigenvalue analysis can be a very powerful tool for identifying particular modes of variability in a given set of data. However, EOFs can identify standing oscillations, giving only suggestions of the existence of propagating signals; these can be highlighted by CEOF analysis, which is a technique designed to characterize the propagating modes of variability with a pair of real and imaginary spatial pattern in quadrature with one another (Preisendorfer and Mobley 1988; von Storch and Navarra 1999), a method applied to the study of Rossby waves and basin modes in many previous works (White 2000a, 2004; Santoso and England 2004; Yang et al. 2004). After the CEOFs are computed, the real and imaginary eigenvectors, together with their eigenvalues, can be manipulated to obtain several useful functions defining the mode evolution in both space and time. We therefore try to identify the periods and spatial characteristics identified so far in both the atmosphere and ocean at the two central latitudes.

Because we are interested in the propagation of Rossby waves only, and we have recognized the main periods involved at both central latitudes, we apply a 1–10-yr bandpass filter to all our variables, filtering out intraannual and interdecadal frequencies before performing the CEOF analysis on our datasets. We will focus on the results at $\phi = 40°$ only, because the results at $\phi = 30°$ are qualitatively similar.

Analyzing the spectra of the principal components (PCs) we can extract the periods of each CEOF mode, and the spatial patterns associated with the main Rossby wave peaks were found to be CEOF-1 and CEOF-2. In Fig. 4 we plot the results of the second CEOF for OCH1, OCH2, and SST. When comparing the real (left panels) and the imaginary (right panels) spatial structures of Fig. 4, the wavenumber-2 westward-propagating Rossby wave is visible in all variables with an apparent baroclinic structure.

But what are the structures dominating the propagating features in the atmosphere? We find that the main atmospheric response in our simulations is a wavenumber-3 wave at all central latitudes. The first two modes in the CEOF analysis are dominated by an annular mode, but CEOF-3 and CEOF-4 (plotted in

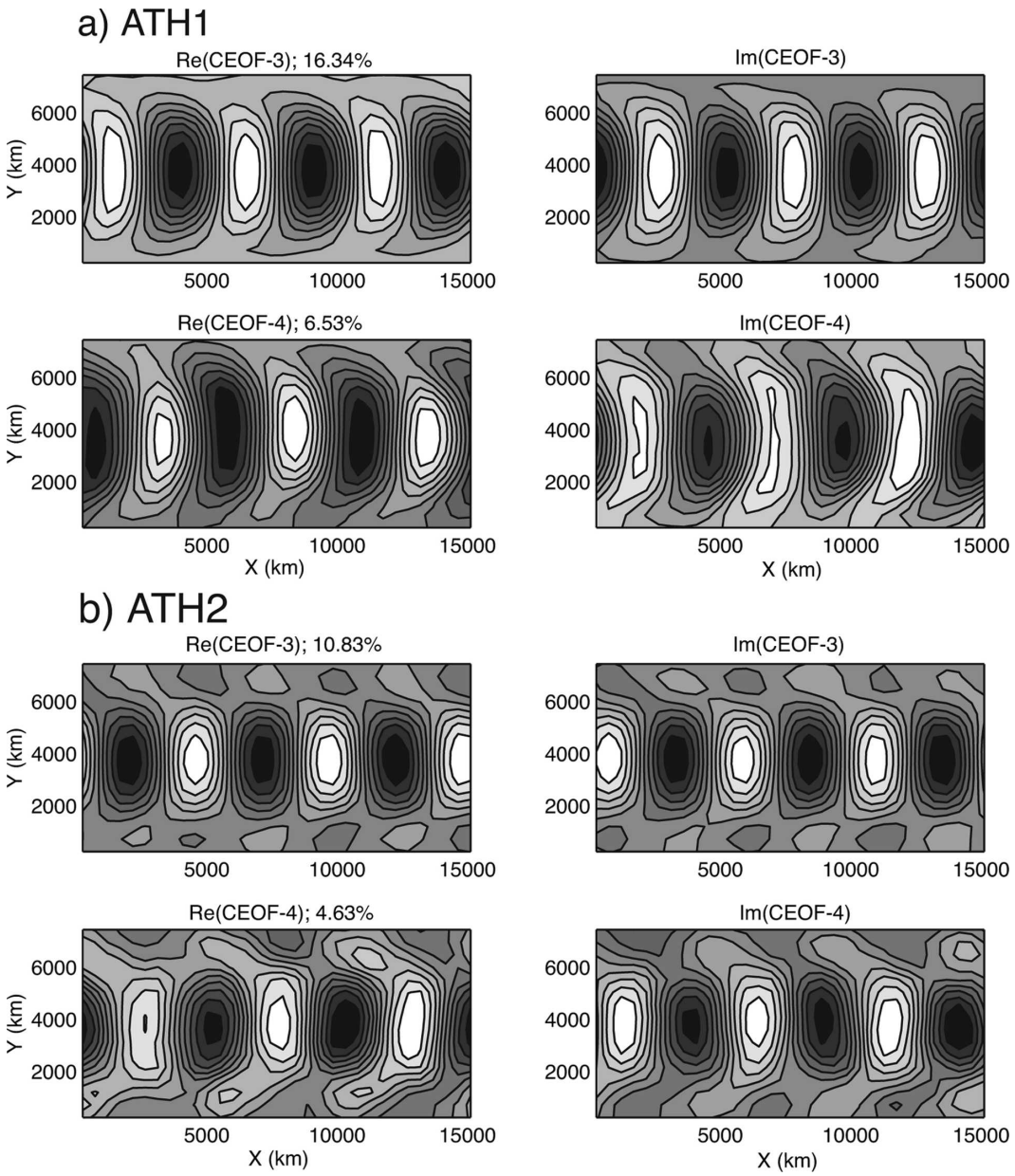

FIG. 5. (left) The real and (right) imaginary (a) CEOF spatial patterns for the first interface height (ATH1): (top) CEOF-3 (16.34%) propagating eastward as a wavenumber-3 wave, and (bottom) CEOF-4 (6.53%) propagating westward as a wavenumber-3 wave. (b) Same as (a), but for the second interface height (ATH2): (top) CEOF-3 (10.83%) propagating eastward as a wavenumber-3 wave, and (bottom) CEOF-4 (4.63%) propagating westward as a wavenumber-3 wave.

Fig. 5 for ATH1 and ATH2) show the wavenumber-3 wave structure with an important and fundamental difference between the two.

The atmospheric interface heights of CEOF-3 show a wavenumber-3 wave with a relatively high percentage of variance (16.34% and 10.83%) propagating eastward. CEOF-4 for both ATH1 and ATH2 explains a much smaller amount of variance in the atmosphere (6.53% and 4.63%), but the same wavenumber-3 wave is observed to travel westward instead (bottom panels of ATH1 and ATH2 in Fig. 5), with an apparent equivalent barotropic structure. The AST has the same response in spatial patterns for both modes (not shown).

The periods of the oceanic and atmospheric modes shown so far are inferred from the spectra of the cor-

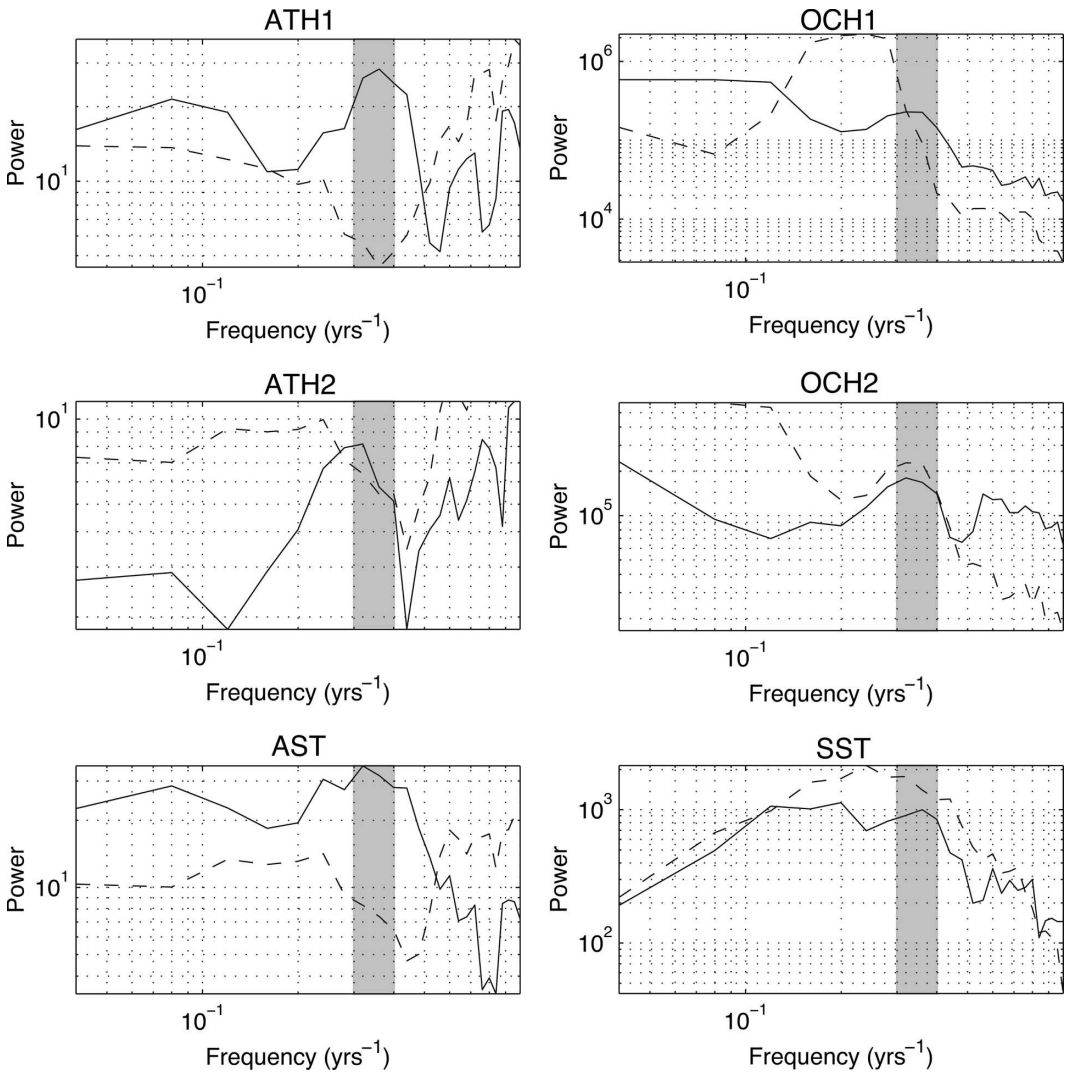

FIG. 6. Normalized spectra of atmospheric and oceanic H1, H2, and surface temperature. (left) Atmospheric spectra: (broken lines) CEOF-3, which is dominated by high frequencies, and (solid lines) CEOF-4, with a common peak at $P \sim 3$ yr. (right) Oceanic spectra: (broken lines) CEOF-1 and (solid lines) CEOF-2, which shares the same peak as the atmospheric CEOF-4. The region of the common peak is highlighted by the gray area in all panels.

respondent PCs. Normalized spectra of atmospheric CEOF-3 and CEOF-4 and oceanic CEOF-1 and CEOF-2 are plotted in Fig. 6. The atmospheric CEOF-3s (broken lines) are dominated by energy at short periods in all three variables and do not seem to share any particular relation with the oceanic spectra of CEOF-1. In contrast, the atmospheric CEOF-4 modes have a clear peak for $P \sim 3$ yr, matching the oceanic CEOF-2 spectra with exactly the same period. The computation of the spatial and temporal phases, extracted from each CEOF mode, confirmed both the sense of propagation and the period of the oscillation of the westward-propagating wave in the ocean and atmosphere. Thus, an atmospheric equivalent barotropic wave, traveling westward with a period of around 3 yr, seems to be coupled with a baroclinic Rossby wave of same period.

Last, we can nicely represent the propagation of the atmospheric and oceanic wave with a sequence of maps, computed at 90° intervals, multiplying the real and imaginary part of the spatial components by the cosine and sine of the phase, respectively, as shown in Fig. 7.

This should be read from top to bottom, following weights of the same sign during the half-cycle evolution. Each variable is initialized with the same arbitrary phase. The oceanic wave is observed to propagate as a wavenumber-2 baroclinic wave with a defined and co-

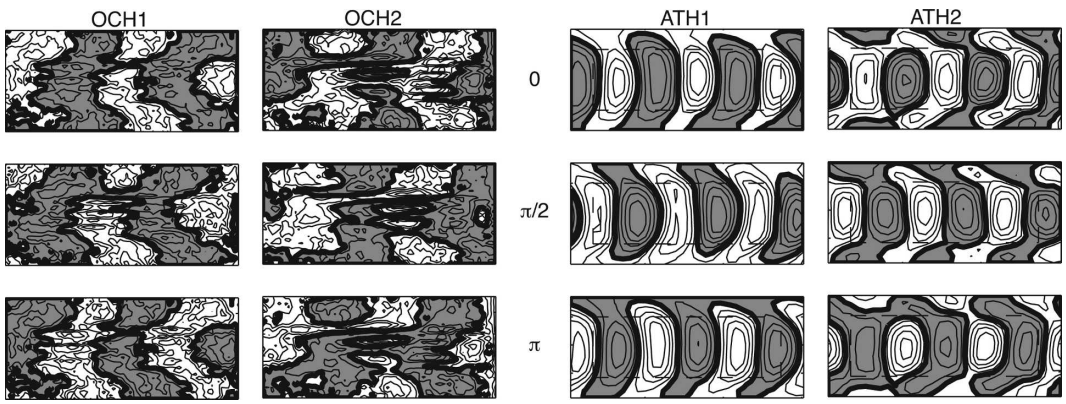

FIG. 7. Phase sequence of (left) the oceanic CEOF-2 and (right) atmospheric CEOF-4 over half a cycle at $\phi = 40°$. The plot should be read from top to bottom, following weights of the similar sign, giving a westward sense of propagation for all variables at approximately the same speed. The rectangular dashed box in the atmospheric panels stands for the ocean basin domain.

herent pattern over the entire basin. The atmospheric wave is instead equivalent barotropic with a wavenumber-3 structure, following the oceanic wave at approximately the same speed. The meridional extension of the atmospheric wave is given by the dimension of the ocean basin, represented by the rectangular dashed box, and oceanic anomalies are observed to be in phase with atmospheric anomalies.

So far, we identified Rossby waves in the Q-GCM traveling faster than the linear theory predicts. After characterizing the oceanic Rossby waves at both central latitudes we looked at the atmospheric response, finding atmospheric waves that are able to propagate westward. The major peaks in the spectra of these waves match the oceanic Rossby wave period. From the statistical eigenanalysis employed, an oceanic wavenumber-2 baroclinic Rossby wave, dominating the frequency–wavenumber spectrum, seems to be coupled with an atmospheric equivalent barotropic wave traveling in phase with the first oceanic interface height. The amplitude of the baroclinic wave is given by the signals identified in the Hovmöller plots, and these are characterized by anomalies of the order of 40 m. On the other hand, the amplitude of the equivalent barotropic atmospheric wave can be inferred from the temporal amplitudes in the CEOF analyses; they reveal anomalies of the interface heights between 100 and 200 m, increasing with height.

Thus, is there a real coupled Rossby mode taking place in this process and is this responsible for the features observed in the oceanic Rossby wave propagation? Following the same technique of analysis pursued in previous sections, we proceed to try correlating the signals identified in the ocean–atmosphere datasets and find a coupled mode of variability associated with the patterns described with standard and complex EOF analysis.

5. The coupled Rossby wave

Canonical correlation analysis (CCA) is a powerful multivariate linear statistical methodology that identifies and isolates correlated patterns between two fields (Bretherton et al. 1992; von Storch and Navarra 1999; von Storch and Zwiers 2001), and is a technique that had been widely used in climatology studies (Barnett and Preisendorfer 1987; Bretherton et al. 1992; Pierce et al. 2001). A way of reducing the intrinsic noise and possible spurious patterns was first proposed by Barnett and Preisendorfer (1987), whereby the CCA is performed after transforming the original fields into an EOF space. Hence, our subset of renormalized leading EOF patterns and PCs are used as a base for CCA.

We will again focus on the results at $\phi = 40°$ discussing only the differences for the other central latitude. We thus perform the CCA on the unfiltered EOFs and compute the first six canonical correlation patterns (CCPs) between all oceanic and atmospheric variables in descending order of importance.

The patterns obtained can be divided into the following two groups: a strong correlation between some oceanic and atmospheric vectors with a baroclinic response in the atmosphere, and a less-strong, but still very significant, correlation where the concept of "equilibration" (Shutts 1987) takes place and the atmosphere is equivalent barotropic. In the latter, quasi-stationary atmospheric waves are forced by an external thermal source, that is, oceanic temperature anomalies, and can actively couple with the oceanic SST giving rise to resonance (Held 1983; Frankignoul 1985). This is exactly

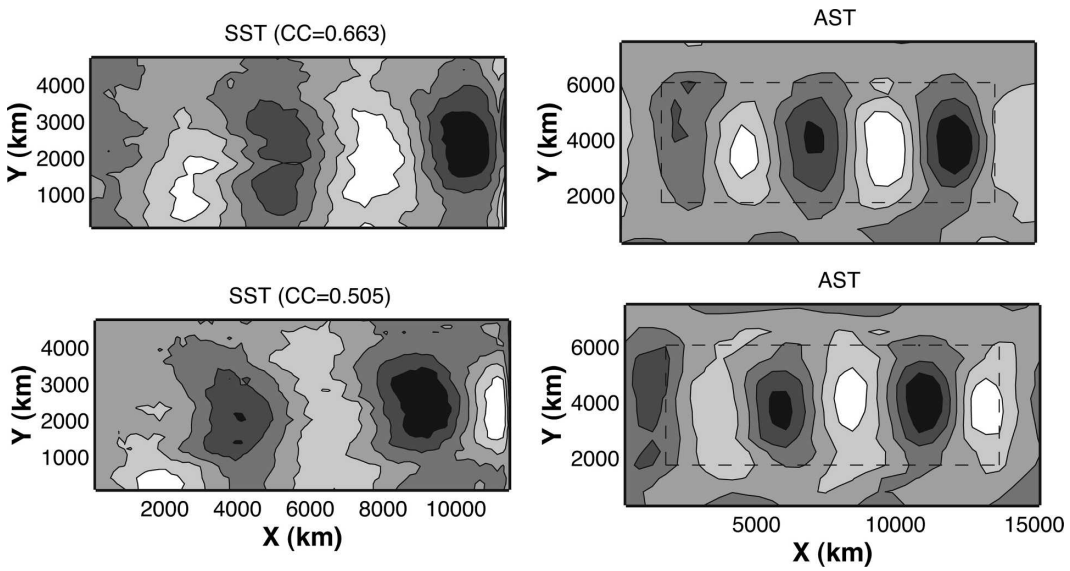

FIG. 8. First two canonical correlation patterns of the SST–AST analysis with their respective canonical correlation values: (left) SST and (right) AST; (top) CCP-2 and (bottom) CCP-2. SSTs are in phase in CCP-2. The rectangular dashed box in the atmospheric panels stands for the ocean basin domain. Negative weights are shaded.

the atmospheric configuration of the fastest-growing mode proposed by GM99, in which high (low) pressure anomalies are associated with warm (cold) SST, growing in amplitude with height.

Baroclinic and equivalent barotropic structures have been both modeled and observed, and an appropriate simulation of the eddy feedback is believed to be crucial for the generation of equivalent barotropic responses, as reviewed by Ferreira and Frankignoul (2005). Moreover, the atmospheric structure is frequency dependent with baroclinic responses dominating at interdecadal periods and equivalent barotropic atmospheres present for interannual periods (Colin de Verdière and Blanc 2001).

In our model, heat flux exchanges between the ocean and atmosphere components are directly expressed through both mixed layers by their respective temperature equations. The correlation between SST and AST is thus expected to be very high because the SST–AST feedback takes place at short time scales and locally in space (Pierce et al. 2001).

Indeed, in Fig. 8 CCP-1 and CCP-2 are characterized by high correlations, and in both modes SSTs are found to be in phase with ASTs.

Figure 9 shows the spectra of CCP-1 (thin line) and CCP-2 (thick line) for the CCA analysis between oceanic and atmospheric temperatures. CCP-1, the strongest correlated pattern, takes place at high frequencies, with peaks at $P = 1.5$ and 2.5 yr, not corresponding to any particular energy peak for Rossby wave propagation at this central latitude. CCP-2 however peaks at $P \sim 3$ yr, exactly like the Rossby wave identified in the CEOF analysis does. We will show that this pattern is repeated in all different CCPs, where the most correlated mode, CCP-1, has a baroclinic atmospheric response at periods unrelated to the main Rossby wave while CCP-2 has an equivalent barotropic atmosphere structure with the oceanic Rossby wave coupled underneath.

At this stage it should be useful to remember the mechanism proposed by GM99 through which they found growing decadal Rossby waves propagating as coupled modes in the ocean–atmosphere system in their idealized analytical study. Their fastest-growing coupled mode was given by the phase relationship schematized in Fig. 10 corresponding to both their "entrainment case" and "advective case." The only situation in which a coupled mode can develop is when the atmosphere is equilibrated, or is in an equivalent barotropic structure, with amplitudes of anomalies increasing with height. High (low) pressures cause anomalous downward (upward) Ekman pumping that deepens (shoals) the first interface height leading to warm (cold) SST anomalies. Therefore, the resulting phase relationships are equivalent barotropic positive pressure anomalies on top of warm SST and downward displacement of OCH1, and the opposite for negative atmospheric pressure anomalies. However, growth can occur between a phase shift of $\pm 90°$, reducing toward quadrature.

GM99 found that both entrainment- and advective-dominated cases were equally important, but the entrainment case produced the biggest growth rate. The

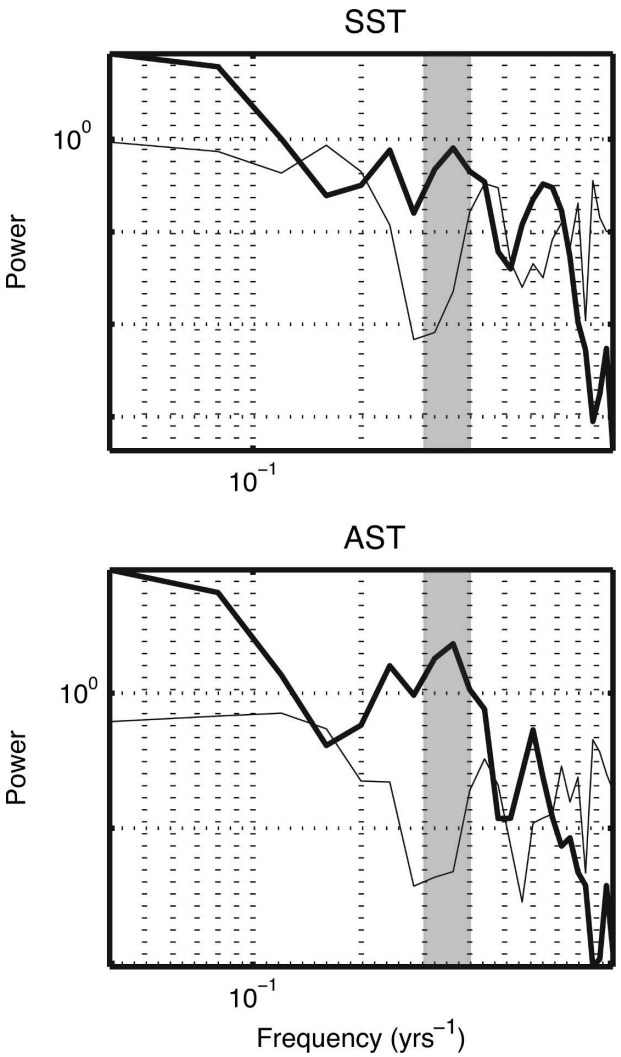

FIG. 9. Spectra of the modes of Fig. 8: (top) SST and (bottom) AST; first (thin line) and second (thick line) modes. The first CCP correlation takes place at short periods, while the second CCP has a definite period of ~3 yr that corresponds to the main Rossby wave propagating at $\phi = 40°$.

advection mechanism, rather than the vertical entrainment, is thought to be both more important and efficient within Rossby wave dynamics, and it has been theorized that anomalous meridional geostrophic advection of SST by westward-traveling Rossby waves is the link in the ocean–atmosphere coupling leading to growing coupled waves (White et al. 1998; White 2000b). Later, we will try to identify which of the two mechanisms is active in our simulations by partially decoupling the SST equation in the ocean.

Inspection of the second CCPs of the SST–ATH1 and SST–ATH2 analyses (Fig. 11) reveals that warm SSTs are indeed underneath low ATH1 (high pressures), and vice versa with an equivalent barotropic atmosphere. This corresponds to the case described by CCP-2 of Fig. 8 in which SSTs are in phase with ASTs and peak at the Rossby wave period. Instead, the first CCP of the SST–ATH1 and SST–ATH2 analysis has a baroclinic atmosphere, corresponding to CCP-1 of Fig. 8 with a clear phase shift between SST and ATH1. In both CCPs, the correlation, given by the canonical correlation coefficients (CCs), is relatively strong.

We observed that phase shifts around 90° between SST and ATH1 occur in CCP-1. Although direct comparisons with, for example, the works of Frankignoul (1985), Shutts (1987), and GM99 can be difficult because of the inclusion of both an atmospheric and an oceanic temperature equation in the Q-GCM, without parameterization of a forcing function as in the aforementioned studies, the phase shift would always imply a baroclinic response in the atmospheric pressure field.

This mode might be associated with the observations of White et al. (1998) and White (2000a), for example, where SST is usually found in quadrature with SLP. However, correlations between oceanic and atmospheric variables are not so coherent and the common spectra usually peak at the annual/biannual period (Fig. 12), where Rossby wave activity is very weak in the model for this latitude.

The spectra for the analyses of SST–ATH1/–ATH2 and SST–ATPA1/–ATPA2, where ATPA is the atmosphere layer pressure, are shown in Fig. 12 and confirm what was previously said for the SST–AST evolution. In all four pairs of spectra the main coupled peak is characterized by a period of 3 yr for the second mode (thick line), while for the first baroclinic mode (thin line) there is evidence of a coupling taking place at both annual/biannual and decadal periods. This might also be related to the interdecadal periods at which the atmosphere responds in a baroclinic way (Colin de Verdière and Blanc 2001). The second strongest relationship between the ocean and atmosphere is then equivalent barotropic. The ocean should always be in a baroclinic state, and the phase relationships between OCH1, OCH2, and atmospheric temperature are well reproduced in the CCA analysis as depicted in Fig. 13. Here the ocean is again baroclinic, resembling the structures identified in Fig. 4 for the Rossby wave. The first ocean interface height is out of phase with the atmospheric temperature because this last is phase locked with SST. The correlation coefficient is diminished for OCH2 but is still significantly high. The corresponding spectra are also analyzed, and while OCH1–AST peaks at the Rossby wave period $P = 3$ yr, we could not find the appropriate peak for the thermocline displacement, possibly because the strength of the correlation was weak in this case. We

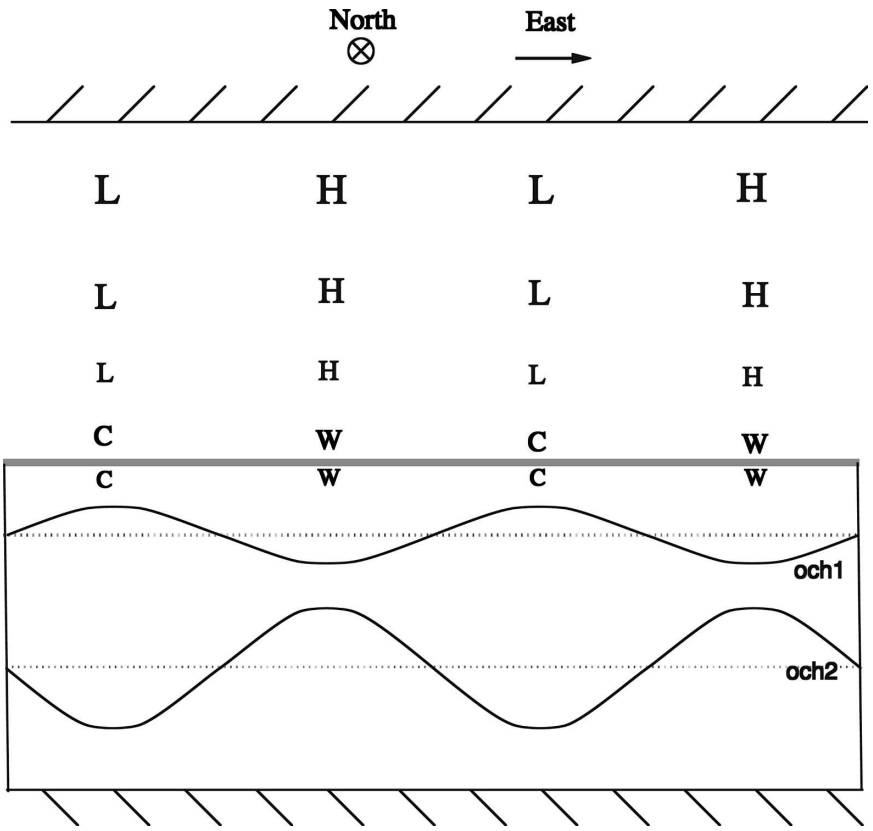

FIG. 10. Phase relationships between ocean and atmosphere for the fastest-growing mode of GM99 extended to our three-layer model (adapted from GM99). Atmospheric pressures are denoted by symbols H and L; the size of the symbols relates to the magnitude of the anomaly. Symbols W and C refer to warm and cold SST while the undulating lines indicate the positions of the oceanic interface heights.

were able to trace the Rossby wave period in the thermocline patterns during other analysis, as, for example, in the canonical correlation of OCH2–ATH1 and OCH2–ATH2 whose spectra are again shown in Fig. 14, although the peak is not as sharp but distributed over a small amount of frequencies. Other results could have been shown but they all reflect the same mechanism and phase relationship previously described.

So far, we have described the behavior of the coupled system at $\phi = 40°$. To include the patterns and spectra for $\phi = 30°$ would have been repetitive most of the time because the main features remain the same; significant differences between the two runs do exist though. The coupled patterns observed when the model is moved toward the equator are less coherent and the correlations are much weaker. The spectra of the canonical analysis still peak at the Rossby wave main period with an equivalent barotropic atmosphere above it, but it is more difficult to differentiate the modes associated with the baroclinic Rossby wave and its relation with the equilibrated atmosphere. This seems to indicate a weaker coupling of the ocean–atmosphere system under the mechanism described for higher latitudes. An explanation might be given by the period of the main ocean wave involved in the coupling. Oceanic Rossby waves have a meridional profile for their zonal phase speed, with westward phase speeds decreasing as the inverse square of the latitude (Gill 1982). It is possible that oceanic Rossby wave speeds, as we move toward the equator, become too fast to maintain the phase relationship necessary to induce the equilibrated atmospheric waves that are able to positively couple with the external thermal forcing. This could also be an explanation for the greater increase in phase speeds found with the FFT analysis at $\phi = 40°$: because the coupling is stronger there, a potential coupling speedup should also be stronger at that latitude.

To test this hypothesis we should perform other runs at different latitudes and confirm whether a band of latitudes at which the coupling is maximized really exists.

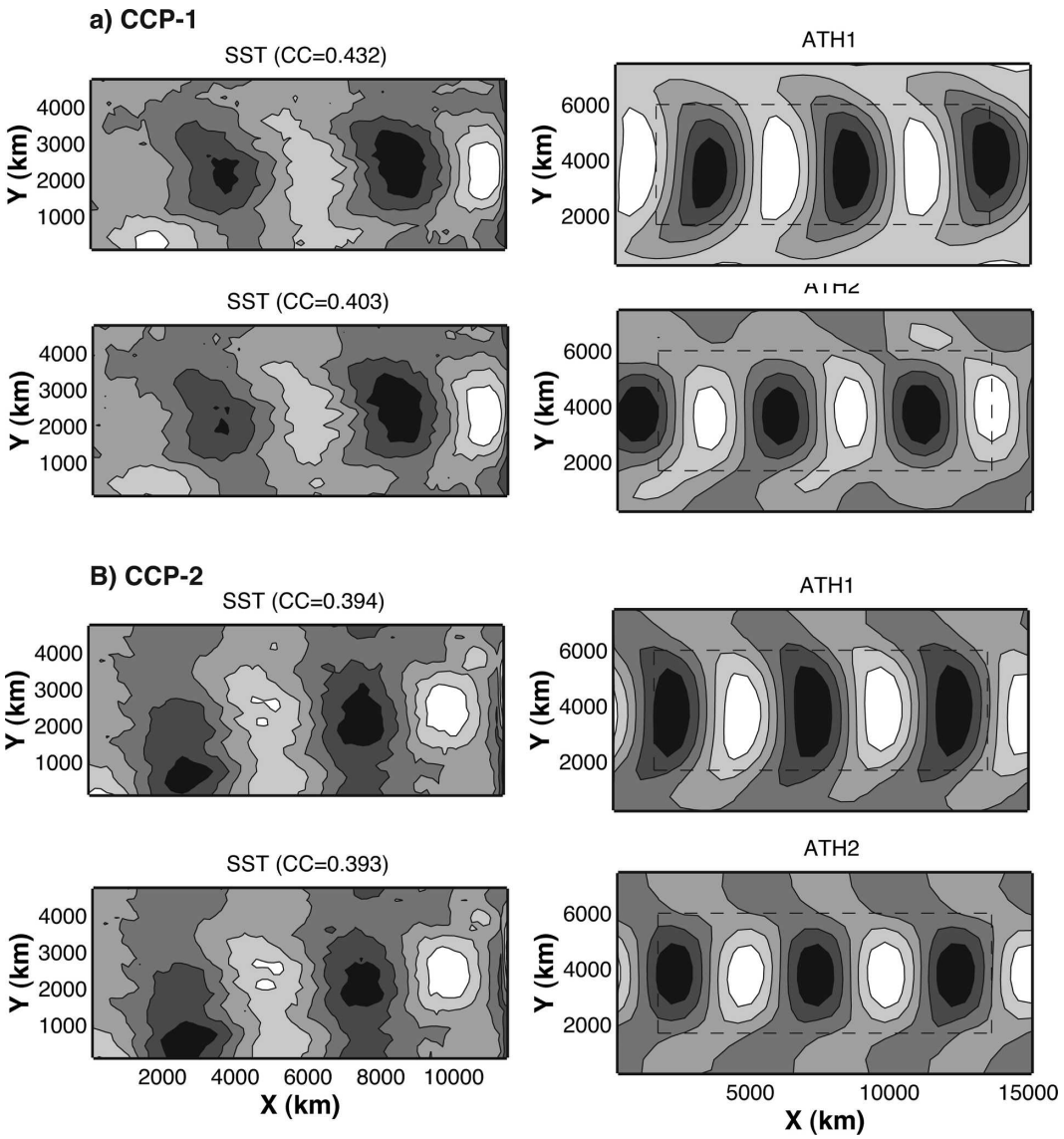

FIG. 11. (left) SST and (right) ATH1 and 2. (a) CCP-1. Warm SSTs are 90° out of phase with high atmospheric pressures but with a phase shift while the atmospheric structure is baroclinic. (b) CCP-2. Warm SSTs are in phase with high atmospheric pressures and negative atmospheric interface heights. The atmospheric structure in the first and second mode, corresponding to the coupled Rossby wave mode, is equivalent barotropic.

a. The importance of horizontal advection and entrainment of temperature anomalies

GM99 proposed two different but equally important mechanisms for the generation of SST anomalies causing a positive ocean–atmosphere feedback. The first is the entrainment mode, in which vertical advection processes during the transit of the oceanic wave generate anomalous warm and cold SSTs. When the atmosphere response is equilibrated, the anomalous Ekman pumping will work to reinforce the SST anomalies and the amplitude of the wave. The second mechanism is the advection mode; in this case the horizontal advection of mean SST by geostrophic flow generated by undulations in the ocean's interfaces is responsible for establishing SST anomalies out of phase with the first interface height. The latter case was involved in the unstable coupled interactions of Qiu et al. (1997) and van der Avoird et al. (2002). For instance, the coupled instability of van der Avoird et al. (2002) was due to horizontal advective processes only, because of neglected entrainment in the ocean.

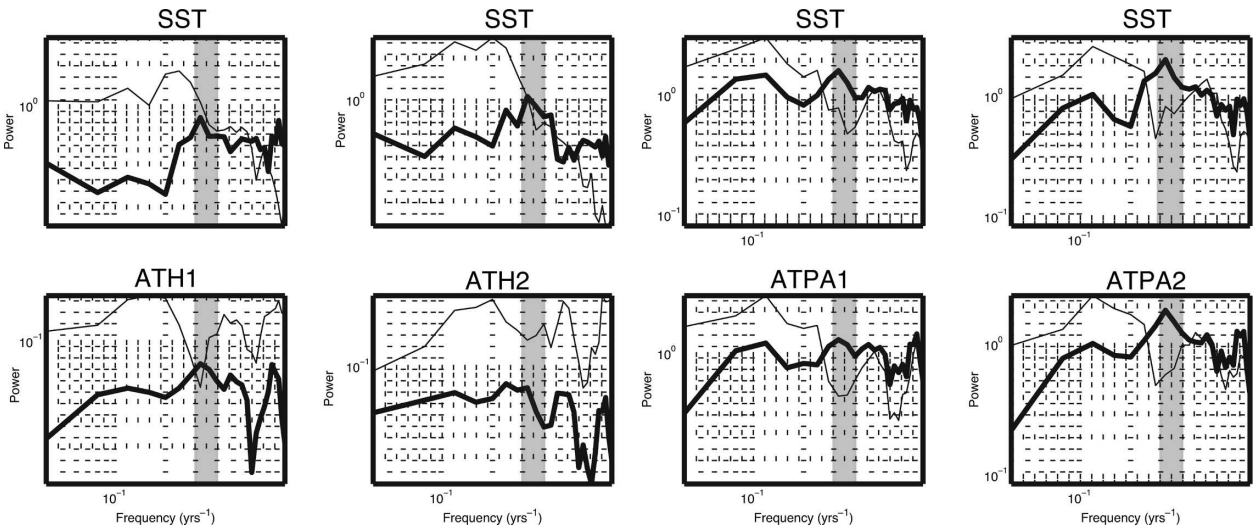

FIG. 12. Normalized spectra of (left to right) SST–ATH1, SST–ATH2, SST–ATPA1, and SST–ATPA2. Thin lines are for CCP-1 and thick lines for CCP-2. The second correlation occurs at $P = 3$ yr between an oceanic baroclinic Rossby wave and equivalent barotropic atmospheric wave. The first correlated pattern seems to happen at 5–10 yr.

By modifying the SST equation in order to suppress one or the other mechanism, we will try to understand which mode is responsible for the couple Rossby wave in our model.

1) THE ENTRAINMENT MODE

We will first eliminate the horizontal advective terms in the SST tendency equation, in this case (2) reduces to the entrainment-only case:

$$\partial_t T = \frac{w_{\text{oek}}}{H_m} T + K_2 \nabla^2 T - K_4 \nabla^4 T - \frac{F_0 - F_m}{\rho_o C_{\text{po}} H_m}. \quad (3)$$

Thus, vertical entrainment through interfaces is still active but the ocean circulation is not able to advect the temperature field. We continued the previous run at $\phi = 40°$ for another 50 yr and investigated the correlation and wave response in all oceanic and atmospheric variables. It could be argued that eliminating

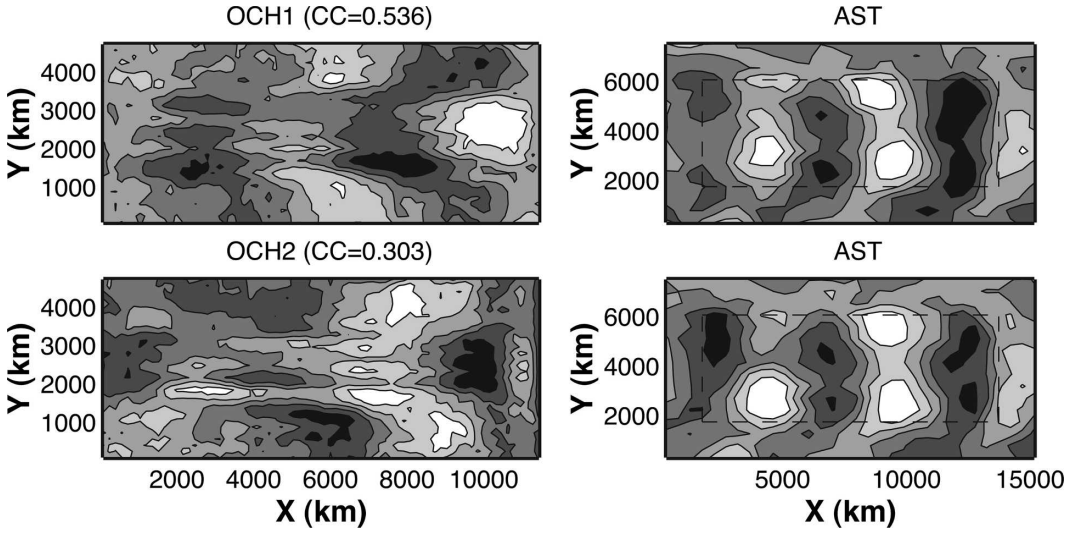

FIG. 13. CCP-2 of the (top) OCH1–AST [correlation coefficient (cc) = 0.536] and (bottom) OCH2–AST (cc = 0.303) correlation. The ocean has a Rossby wave–like structure with cold atmospheric temperature anomalies over positive interface anomalies.

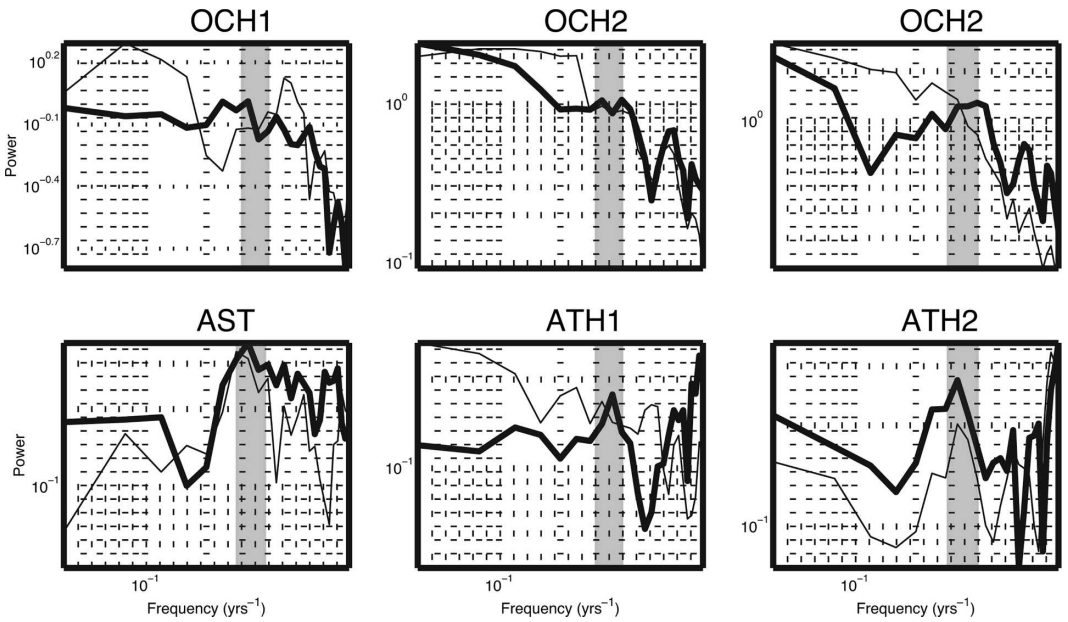

FIG. 14. Normalized spectra for CCP-1 (thin line) and CCP-2 (thick line) of the (left) OCH1–AST, (middle) OCH2–ATH1, and (right) OCH2–ATH2 correlation analyses.

advection of SST might have significant consequences in the atmospheric mean state and, in turn, that the resulting wind stress might significantly differ. This could prevent quantitative comparisons between the fully coupled and the entrainment-only wave response, but the qualitative results will hold.

The spatial patterns of the second most correlated mode between SST, ATH1, and ATH2 are shown in Fig. 15. The SST patterns are much smoother but still resemble the patterns related to the Rossby wave propagation plotted in Fig. 11 for CCP-2. Also, the atmospheric response is again a wavenumber-3 equilibrated wave. The spatial relationship between the different variables is maintained for the coupled Rossby mode with the same shared peak at $P \sim 3$ yr (not shown). Only the correlation coefficients are significantly different, having decreased, for the case shown, to 0.350 for the SST–ATH1 analysis and 0.292 for the SST–ATH2 analysis.

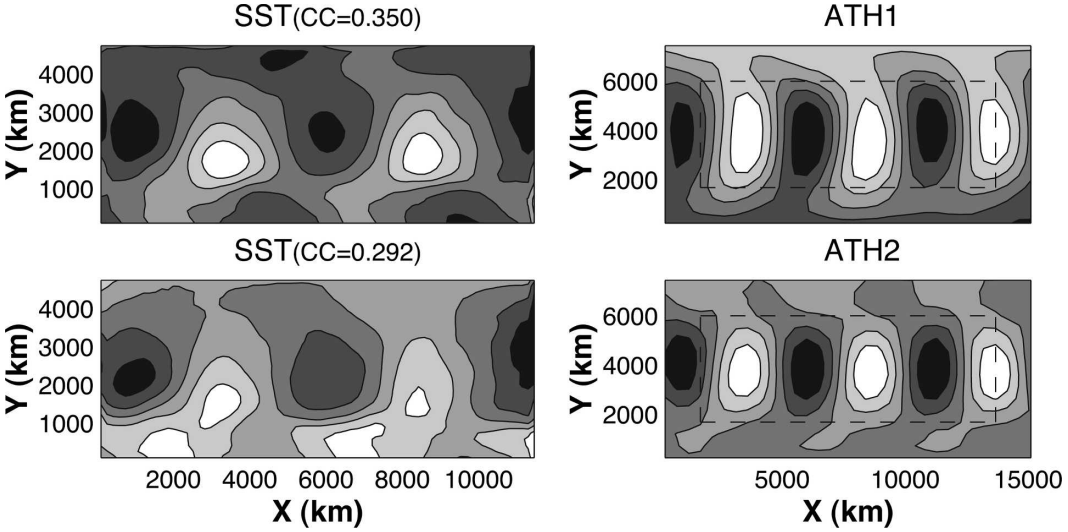

FIG. 15. Second canonical correlation patterns of (top) SST–ATH1 and (bottom) SST–ATH2 for the case with no advection of oceanic temperature anomalies. Phase relationships are conserved and the atmospheric response is equivalent barotropic. However, correlation coefficients are weaker (SST–ATH1, cc = 0.350, SST–ATH2, cc = 0.292).

The spectra of the PCs reveal the existence of the Rossby wave peak in both the oceanic and atmospheric variables with little difference with the case for the full-SST equation. Indeed, in Fig. 16 the spectra of the first (thin lines) and second (thick lines) CCP of the SST–ATH1 and SST–ATH2 analyses are plotted: the shared Rossby peak is strong in the oceanic temperature and atmospheric heights while there has been an increase in the variance at lower frequencies.

Overall, the results obtained with the entrainment-only SST equation are very similar to the full-SST analyses and the coupled Rossby wave is still generated with similar characteristics without the horizontal advection of temperature anomalies. This result underlines the importance of the entrainment processes of SST for the generation and maintenance of the coupled mode, while not requiring advection by the ocean circulation. However, the correlation between the ocean and atmosphere in the coupled mode are much weaker, indicating that when both horizontal and vertical processes are present they mutually work to reinforce the equilibrated atmospheric response and the resulting positive feedback.

2) THE ADVECTIVE MODE

To suppress entrainment in the mixed layer and retain horizontal advective processes only, entrainment heat fluxes are set to zero and (2) now reads

$$\partial_t T + \mathbf{u} \cdot \boldsymbol{\nabla} T = K_2 \nabla^2 T - K_4 \nabla^4 T - \frac{F_0}{\rho_o C_{\mathrm{po}} H_m}. \quad (4)$$

Similarly, as for the entrainment mode case, we continued the run for 50 yr and the results of the CCA analyses between SST and ATH1–ATH2 are shown in Fig. 17.

There is no trace left of the equilibrated response in the atmosphere and the two most correlated pattern show a baroclinic atmospheric wave with high correlation coefficients. The spectra of the first four most correlated patterns (bottom panels of Fig. 17) reveal no peak at the Rossby wave period for ATH1 and ATH2.

Therefore, we conclude that the advective mode alone is not able to sustain the coupled Rossby wave in our model and only in the presence of entrainment processes can the coupled oscillation develop. Following these results we believe that entrainment fluxes in the ocean cannot be neglected, as some authors did (Qiu et al. 1997; van der Avoird et al. 2002), if a coupled instability of the GM99 type is pursued.

b. A forced solution

To test the previous hypotheses that the coupled feedback between the oceanic Rossby wave and the

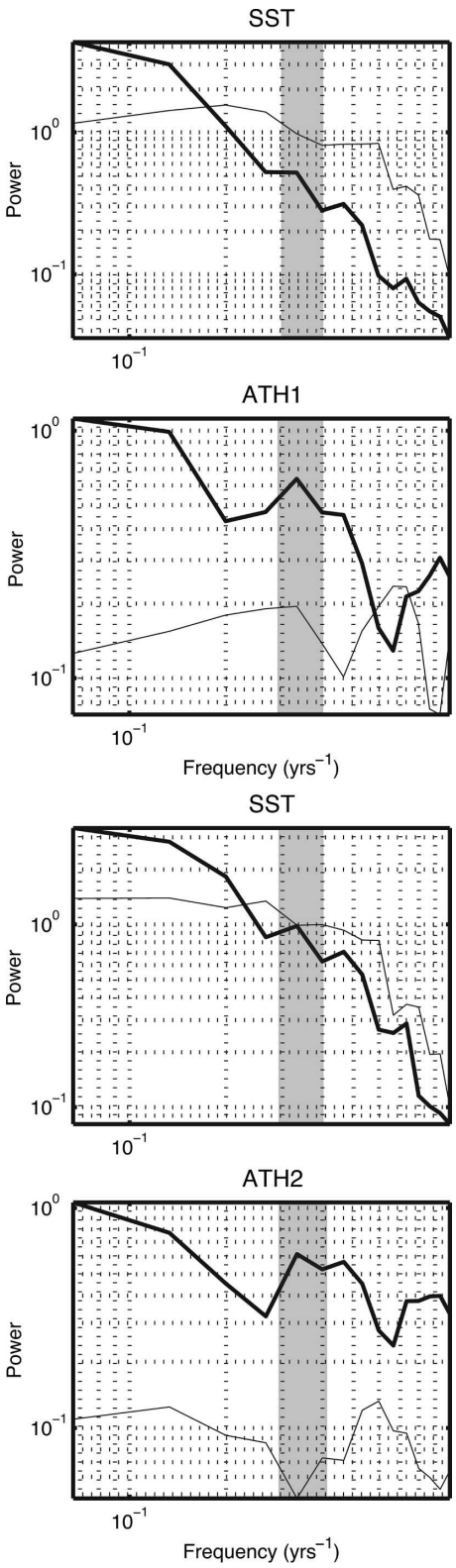

FIG. 16. Spectra of the (top two panels) SST–ATH1 and (bottom two panels) SST–ATH2 canonical correlation analyses for CCP-1 (thin lines) and CCP-2 (thick lines) of Fig. 15. The shaded area in all plots ranges between 0.3 and 0.4 s^{-1} and highlights the common Rossby peak at $P = 3$ yr.

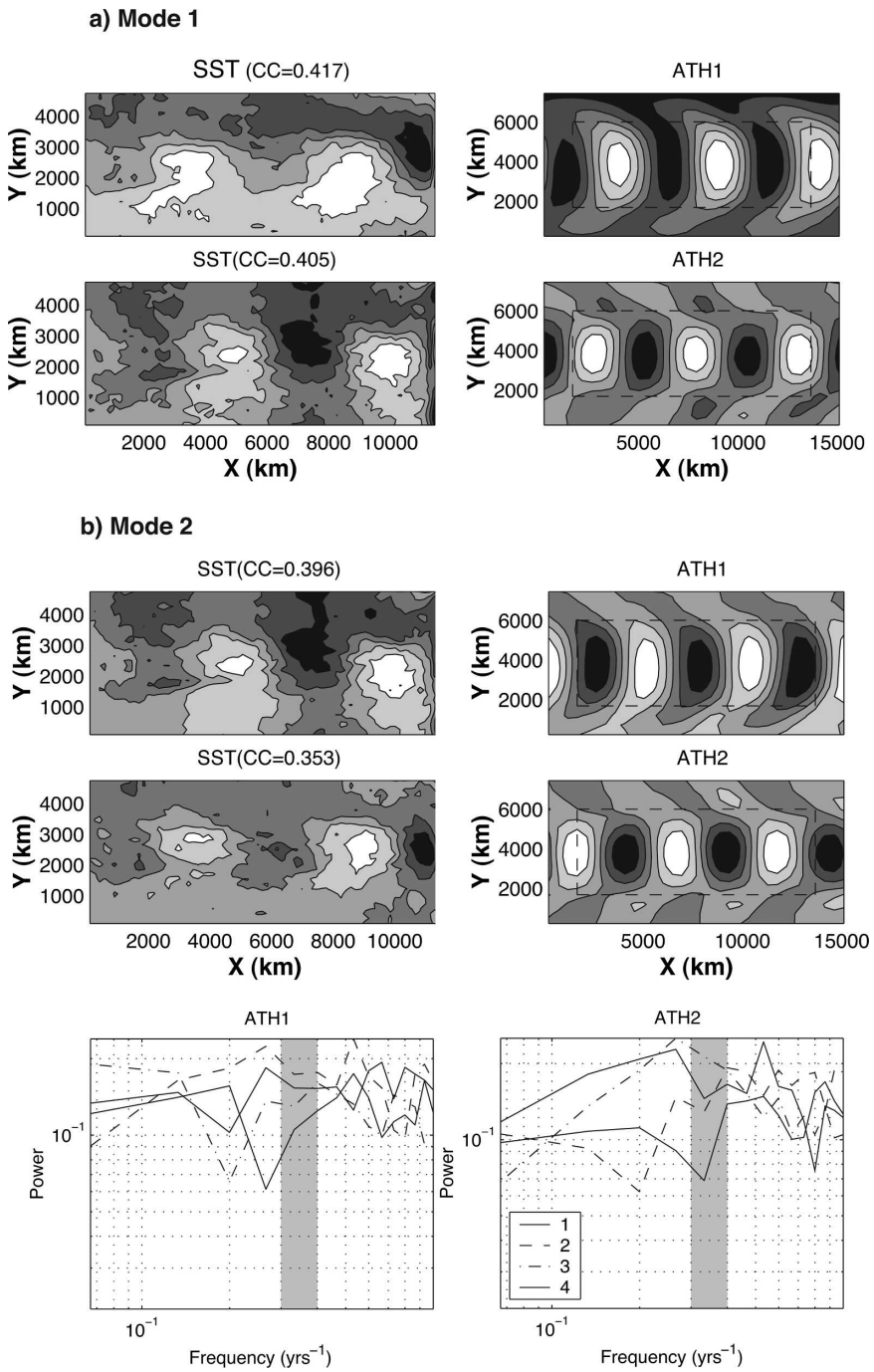

FIG. 17. First two most correlated patterns of the SST–ATH1 and SST–ATH2 CCA for the advective-only SST: (a) CCP-1 and (b) CCP-2. Both CCP-1 and CCP-2 show a baroclinic response in the atmosphere and the equivalent barotropic structure is absent in the remaining modes. (bottom) The ATH1 and ATH2 spectra of the first four modes do not peak at the Rossby wave period as expected.

equilibrated atmosphere can induce changes in the Rossby wave phase speed, we employed the Q-GCM in an ocean-only configuration. The ocean is forced by climatological winds and heat fluxes computed from the previous coupled simulations; the runs are continued for an extra 150 model years and the Rossby wave response is analyzed in a *forced*, not a *coupled*, framework.

The FFT analyses of the westward-filtered OCH2 from the forced runs reveal a significant slowdown of the Rossby wave speed (Fig. 18). While the wavelength of the main peaks remain similar to the coupled runs, the frequencies have clearly diminished resulting, for both central latitudes, in slower phase speeds that are now very close to the perturbed dispersion relation. To allow comparison, the position of the main Rossby peak in the coupled runs is indicated by a black circle.

Thus, Rossby waves, when coupled to the atmosphere with the mechanism described in the previous sections, receive a positive feedback with the equivalent barotropic atmospheric wave inducing an extra speedup, which is added to the one generated by the vertical mean shear.

6. Summary and conclusions

Rossby waves have been studied in the framework of a quasigeostrophic coupled ocean–atmosphere model. The model configuration has three layers in both the oceanic and atmospheric component, the horizontal resolution in the ocean basin is relatively coarse (Δx = 40 km) and viscosities between layers are chosen to be as low as possible. The oceanic domain was chosen to be relatively wide, resulting in a "Pacific like" basin of ~11 500 km.

The characteristics of Rossby waves in the ocean and atmosphere have been identified with statistical eigenvalue techniques for the two central latitudes considered (ϕ = 30° and 40°). An equivalent barotropic atmospheric wave was found to travel westward with similar periods as, and in phase lock with, the oceanic baroclinic Rossby wave, suggesting a coupling between the two. Linear nearly stationary equivalent barotropic atmospheric waves can be generated by, for example, a thermal forcing (Held 1983); in a coupled system these equilibrated waves can represent the quasi-stationary atmospheric waves that couple with the oceanic SST anomalies (Frankignoul 1985; GM99; Colin de Verdière and Blanc 2001; Kravtsov et al. 2005).

Following a statistical correlation analysis, a clear coupled Rossby wave mode, coherent in all oceanic and atmospheric variables was found. The coupled Rossby wave mode has spatial characteristics and periods of the main baroclinic oceanic Rossby waves in the system and resembles the unstable coupled mode mechanism proposed by GM99. Other air–sea phase relationships were observed. For instance, an atmospheric response with high SLP 90° eastward of its SST source, similar to the White et al. (1998) and White (2000b) observations was also identified; however, this was less coherent between the different atmospheric and oceanic variables and was associated with periods other than the main Rossby wave peak in the FFT analysis.

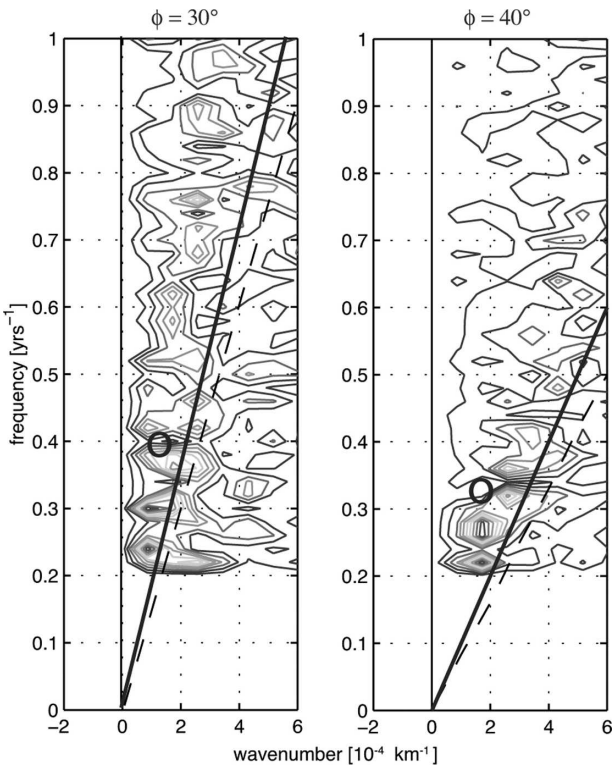

FIG. 18. Fast Fourier transform of the westward-filtered OCH2 in the forced runs at (left) ϕ = 30° and (right) ϕ = 40°. The Rossby wave main peaks are considerably slower than in the coupled runs, of which the main peaks are drawn with a black circle. Solid and dashed lines are as in Fig. 3.

The correlation coefficients of the coupled mode are generally stronger for the case at ϕ = 40° and the spatial structures are also more coherent. This is a possible indication that coupled Rossby modes are more likely to develop as we move poleward. Rossby wave phase speed in the ocean slows down with increasing latitude and positive phase relationships with the quasi-stationary atmospheric response are possible, because slowly propagating waves have more time to develop SST anomalies that will in turn influence the overlying atmosphere. Also, when the coupled mode was tested on the tridimensional resolution and dimensions of the ocean basin (the model was run with a 10-km horizontal resolution six-layer ocean with the zonal extension reduced to 1/3), it proved to be robust to any changes.

We thus argue that a positive feedback is taking place whereby oceanic Rossby waves are efficiently coupled with an atmospheric equilibrated wave traveling in phase and with the period of the oceanic wave. Moreover, partially decoupling the SST tendency equation, the coupled Rossby mode existence has been proved to

depend on entrainment processes of SST anomalies, whereas horizontal advection of temperature anomalies would only strengthen the mechanism.

Whether the coupled mode is ocean or atmosphere driven is difficult to say from this kind of analysis. GM99 proposed as a source of energy for the development of the coupled mode the release of available potential energy (APE) in the ocean, whereby the atmosphere transforms thermal energy stored in the thermocline to mechanical energy through wind stress. Colin de Verdière and Blanc (2001) instead suggested the atmospheric APE as a source of energy in its thermal resonance process. Which of these is happening in our modeling study could be inferred by studying the down-gradient wave heat fluxes in the atmosphere and ocean, as suggested in Colin de Verdière and Blanc (2001).

In a similar study, Kravtsov et al. (2006) found an interdecadal coupled Rossby mode propagating westward with a time scale given by the crossing time of the oceanic Rossby wave. Using a lagged covariance analysis regressing oceanic and atmospheric fields onto ocean kinetic energy they argued that because the SST were larger than the AST anomalies, the mode was forced by the ocean and the APE was released from the thermocline in a similar way as that in GM99. From the CCA analysis depicted in Fig. 8 AST anomalies seem slightly larger than SST anomalies, possibly suggesting that the source of energy in our case is in the atmosphere.

The positive coupling with the atmosphere is able to give an extra speedup other than the baroclinic main flow effect, because the Rossby waves were found to travel faster than the phase speed computed with the inclusion of the mean zonal flow. The calculations of the perturbed dispersion relations are roughly in agreement with the speed-up values given by de Szoeke and Chelton (1999) for our parameter values and show speedups of around 1.2, whereas the coupled Rossby waves are observed to propagate at about twice the unperturbed phase speed. We showed that, when the ocean is simply forced at the surface by winds and heat fluxes with no ocean–atmosphere feedback, these peaks appear at lower frequencies close to the perturbed dispersion relation, indicating that the coupling is indeed a possible mechanism in the speedup of the observed Rossby waves. Last, coupling speedups are observed to be greater for higher latitudes, because the coupled Rossby wave is stronger there.

Increased phase speeds resulting from atmospheric coupling have been suggested in different works (White et al. 1998; Ferreira et al. 2001; Colin de Verdière and Blanc 2001). For instance, White et al. (1998) proposed a zonal and meridional coupling speed resulting from the interaction between the SST field, generated by meridional advection, and the meridional wind anomalies. This extra phase speed was linearly added to the uncoupled linear wave, resulting in significant speedups at middle and high latitudes. This seems to agree with our results, because a higher increase in phase speeds is observed for higher latitudes. In a later study, White (2000a) studied the coupled response at latitudes lower than 30°, suggesting entrainment processes controlling the negative feedback between SST and the atmospheric response resulting in slower phase speeds. The negative feedbacks proposed in White (2000a) are taking place closer to the equator and are not reproducible in our QG coupled model. However, a more detailed study of the latitudinal response, ranging from, for example, 25° to 50°, would give us a stronger indication of any variation in the strength of the coupling and subsequent effects in the Rossby wave phase speeds.

Statistical eigentechniques have been useful in the identification of the properties of both oceanic and atmospheric waves. We were also able to characterize the coupled Rossby wave with its spectral and spatial components. However, we do not know if this coupled mode is unstable, and at this stage we can only speculate on its most important feature, arguing that the mode is weakly damped, with a decaying rate diminished by the coupling. This would agree with what Goodman and Marshall (2003) obtained after the inclusion of oceanic meridional boundaries in the GM99 original model. They could still identify the presence of the coupled mode, but in this case it was found to be weakly damped as a result of the reflection of Rossby waves at the western boundary.

The results presented here are encouraging evidence of the existence of such a Rossby wave coupled mode. However, the model employed is still very idealized and only the analysis of a coupled general circulation model will tell us if this mechanism can be supported together with others that already have some observational basis.

In the meanwhile, to corroborate and shed more light onto the results obtained, a linear stability analysis is proposed as the continuation of this study. It is hoped that the coupled Rossby wave patterns will be reproduced and its eigenspectra will give us information on changes in both frequency and decay/growth rates when different mean states are tested as well as the sensitivity to different parameters. Both proposed studies are currently under way.

Acknowledgments. This study is part of the author's Ph.D. work at the University of Southampton, National

Oceanography Centre, Southampton, Southampton, United Kingdom. Peter Killworth and Jeff Blundell are thanked for their advice and help during this study. Paolo Cipollini and Andy Hogg provided some of their statistical codes and helpful discussions.

APPENDIX

Rossby Waves in the Q-GCM Zonal Mean Flow

The dispersion relation of Rossby waves embedded in zonal mean flows is a standard problem, and full derivations of the normal modes in mean flows are given by several authors (Leblond and Mysak 1978; Pedlosky 1987; de Szoeke and Chelton 1999).

We are interested in whether the Rossby wave activity observed in the quasigeostrophic coupled model is mainly explained by the inclusion of a mean zonal flow in the phase speed calculation. The effect of a baroclinic mean flow on the phase speed of planetary waves has been tackled by many theoretical studies (e.g., Killworth et al. 1997; Dewar 1998; de Szoeke and Chelton 1999; Colin de Verdière and Tailleux 2005). However, we will not attempt to do a thorough study on this subject, which would include taking into account boundary layers, short-wave propagation, the presence of advective modes, and other effects that are still currently being investigated. Here, we will use standard QG theory and derive the dispersion relation of a Rossby wave in a three-layer model in the presence of a zonal mean flow taken from the model employed in this study. The typical vertical shear found by meridional density sections at the latitudes considered here is the one found in the northern part of the subtropical gyre, and this was also the example proposed in the study of de Szoeke and Chelton (1999). This is the location were the Hovmöller plots where constructed in the previous sections and thus it will be the one considered in the comparisons with the phase speeds observed in the model.

Looking for disturbances of a purely zonal flow, $\psi_n = \Psi_n(y) + \phi_n(x, y, t)$, and seeking solutions of the form $\phi = \hat{\phi}e^{i(kx-\sigma t)}$, the standard problem reduces to

$$(kU_1 - \sigma)[-k^2\phi_1 + F_{11}(\phi_2 - \phi_1)] + k\phi_1\partial_y\Pi_1 = 0, \tag{A1}$$

$$(kU_2 - \sigma)[-k^2\phi_2 + F_{21}(\phi_1 - \phi_2) + F_{22}(\phi_3 - \phi_2)] + k\phi_2\partial_y\Pi_2 = 0, \text{ and} \tag{A2}$$

$$(kU_3 - \sigma)[-k^2\phi_3 + F_{32}(\phi_2 - \phi_3)] + k\phi_3\partial_y\Pi_3 = 0. \tag{A3}$$

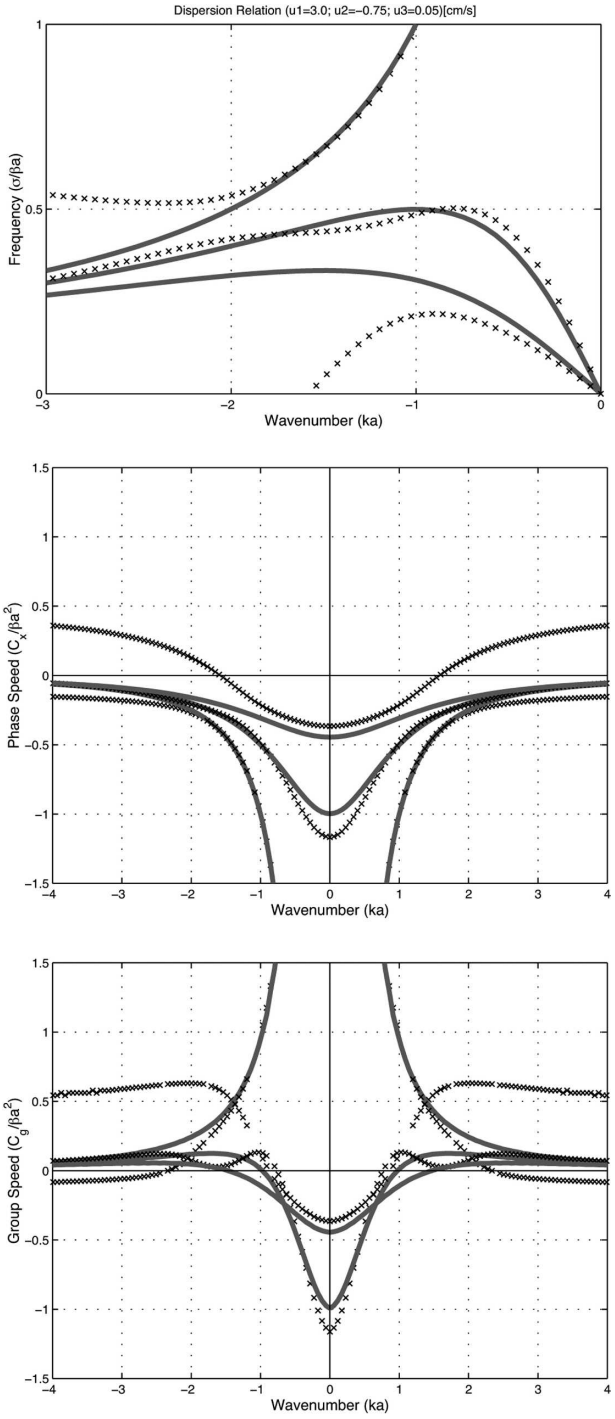

FIG. A1. (top) Dispersion relation, (middle) phase speed, and (bottom) group velocity of the barotropic, and first and second baroclinic mode in the perturbed (times signs) and unperturbed (solid lines) cases. The perturbed solutions are for a vertical shear taken in the northern part of the subtropical gyre, typical for the latitudes considered, and where the Rossby wave characteristics in the model were identified. Mean zonal flow values are $u_1 = 3.0$, $u_2 = -0.75$, $u_3 = 0.05$ cm s^{-1}.

Here U_i and $\partial_y \Pi_i$ are the layer's zonal mean flows and meridional PV gradients, respectively.

The above equations can be cast into a generalized eigenvalue problem of the form $\mathbf{A\Phi} = \sigma\mathbf{B\Phi}$, where $\mathbf{\Phi} = [\phi_1, \phi_2, \phi_3]$ are the eigenvectors and σ is the eigenfrequency. Thus, for different mean flows U_i, we will be able to study the wave response in terms of its perturbed dispersion relation.

The barotropic, and first and second baroclinic mode dispersion relations for the selected case are plotted in Fig. A1. In general, small speedups of the first baroclinic mode are found, especially in the long-wave limit. However, negative effects on the second baroclinic mode and significant modifications in the behavior of the barotropic mode for short wave are evident.

In their study, de Szoeke and Chelton (1999) suggested that in a QG layered system the speedup of the planetary wave propagation speed is a function of the layer depths H_i and the density difference ratio. The mechanism proposed by de Szoeke and Chelton (1999) would indicate for our parameter values a speedup of about 1.4 (their Fig. 4). In our calculations we found a variable speedup/slowdown depending on the wavelength; for the long-wave region that characterizes the Rossby waves observed in the model, we found a maximum speedup of about 1.2. This is the solution plotted as solid lines in Fig. 3.

The choice of layer depths, density jumps, and corresponding Rossby radii are therefore crucial in the resulting Rossby wave phase speed if these are to be compared with real data and if a true estimate is attempted. However, the purpose of this exercise is to estimate the wave speed in the model employed, where a particular mean flow on a flat-bottomed ocean is present, given by the slopes of the interfaces for specific parameter settings.

REFERENCES

Arzel, O., and T. Huck, 2003: Decadal oscillations in a simplified coupled model due to unstable interactions between zonal winds and ocean gyres. *Dyn. Atmos. Oceans,* **37,** 245–270.

Barnett, T., and R. Preisendorfer, 1987: Origins and levels of monthly and seasonal forecast skill for United States air temperature determined by canonical correlation analysis. *Mon. Wea. Rev.,* **115,** 1825–1850.

Barsugli, J. J., and D. S. Battisti, 1998: The basic effects of atmosphere–ocean thermal coupling on midlatitude variability. *J. Atmos. Sci.,* **55,** 477–493.

Bretherton, C. S., C. Smith, and J. M. Wallace, 1992: An intercomparison of methods for finding coupled patterns in climate data. *J. Climate,* **5,** 541–560.

Cessi, P., and F. Paparella, 2001: Excitation of basin modes by ocean-atmosphere coupling. *Geophys. Res. Lett.,* **28,** 2437–2440.

Chelton, D. B., and M. G. Schlax, 1996: Global observations of oceanic Rossby waves. *Science,* **272,** 234–238.

Cipollini, P., D. Cromwell, G. D. Quartly, and P. G. Challenor, 2000: Remote sensing of extra-tropical Rossby waves. *Satellites, Oceanography and Society,* D. Halpern, Ed., Elsevier Science, 99–123.

Colin de Verdière, A., and M. Blanc, 2001: Thermal resonance of the atmosphere to SST anomalies. Implications for the Antarctic circumpolar wave. *Tellus,* **53A,** 403–424.

——, and R. Tailleux, 2005: The interaction of a baroclinic mean flow with long Rossby waves. *J. Phys. Oceanogr.,* **35,** 865–879.

Deser, C., and M. Blackmon, 1993: Surface climate variations over the North Atlantic Ocean during winter: 1900–1989. *J. Climate,* **6,** 1743–1753.

de Szoeke, R. A., and D. B. Chelton, 1999: The modification of long planetary waves by homogeneous potential vorticity layers. *J. Phys. Oceanogr.,* **29,** 500–511.

Dewar, W. K., 1998: On "too fast" baroclinic planetary waves in the general circulation. *J. Phys. Oceanogr.,* **28,** 1739–1758.

Ferreira, D., and C. Frankignoul, 2005: The transient atmospheric response to midlatitude SST anomalies. *J. Climate,* **18,** 1049–1067.

——, ——, and J. Marshall, 2001: Coupled ocean–atmosphere dynamics in a simple midlatitude climate model. *J. Climate,* **14,** 3704–3723.

Frankignoul, C., 1985: Sea surface temperature anomalies, planetary waves, and air-sea feedback in the middle latitudes. *Rev. Geophys.,* **23,** 357–390.

——, P. Müller, and E. Zorita, 1997: A simple model of decadal response of the ocean to stochastic wind forcing. *J. Phys. Oceanogr.,* **27,** 1533–1546.

——, E. Kestenare, N. Sennechael, G. de Cöetlogon, and F. D'Andrea, 2000: On decadal-scale ocean-atmosphere interactions in the extended ECHAM1/LSG climate simulation. *Climate Dyn.,* **16,** 333–354.

Gallego, B., and P. Cessi, 2000: Exchange of heat and momentum between the atmosphere and the ocean: A minimal model of decadal oscillations. *Climate Dyn.,* **16,** 479–489.

Gill, A. E., 1982: *Atmosphere–Ocean Dynamics.* International Geophysics Series, Vol. 30, Academic Press, 662 pp.

Goodman, J., and J. Marshall, 1999: A model of decadal middle-latitude atmosphere–ocean coupled modes. *J. Climate,* **12,** 621–641.

——, and ——, 2003: The role of neutral singular vectors in midlatitude air–sea coupling. *J. Climate,* **16,** 88–102.

Held, I., 1983: Stationary and quasi-stationary eddies in the extratropical troposphere: Theory. *Large-Scale Dynamical Processes in the Atmosphere,* R. P. Pearce and B. J. Hoskins, Eds., Academic Press, 127–168.

Hogg, A., J. Blundell, W. Dewar, and P. Killworth, 2003a: Formulation and users guide for Q-GCM (version 1.0). Southampton Oceanography Centre Internal Document 88, 40 pp.

——, W. Dewar, P. Killworth, and J. Blundell, 2003b: A quasi-geostrophic coupled model: Q-GCM. *Mon. Wea. Rev.,* **131,** 2261–2278.

——, ——, ——, and ——, 2006: Decadal variability of the midlatitude climate system driven by the ocean circulation. *J. Climate,* **19,** 1149–1166.

Jin, F.-F., 1997: A theory of interdecadal climate variability of the North Pacific ocean–atmosphere system. *J. Climate,* **10,** 1821–1835.

Killworth, P. D., and J. R. Blundell, 2005: The dispersion relation

for planetary waves in the presence of mean flow and topography. Part II: Two-dimensional examples and global results. *J. Phys. Oceanogr.,* **35,** 2110–2133.

——, D. B. Chelton, and R. A. de Szoeke, 1997: The speed of observed and theoretical long extratropical planetary waves. *J. Phys. Oceanogr.,* **27,** 1946–1966.

Kravtsov, S., and A. Robertson, 2002: Midlatitude ocean-atmosphere interaction in an idealized coupled model. *Climate Dyn.,* **19,** 693–711.

——, ——, and M. Ghil, 2003: Low-frequency variability in a baroclinic β-channel with land–sea contrast. *J. Atmos. Sci.,* **60,** 2267–2293.

——, ——, and ——, 2005: Bimodal behavior in the zonal mean flow of a baroclinic β-channel model. *J. Atmos. Sci.,* **62,** 1746–1769.

——, P. Berloff, W. K. Dewar, M. Ghil, and J. C. McWilliams, 2006: Dynamical origin of low-frequency variability in a highly nonlinear midlatitude coupled model. *J. Climate,* **19,** 6391–6408.

Kushnir, Y., 1994: Interdecadal variations in the North Atlantic sea surface temperature and associated atmospheric conditions. *J. Climate,* **7,** 141–157.

——, and I. Held, 1996: Equilibrium atmospheric response to North Atlantic SST anomalies. *J. Climate,* **9,** 1208–1220.

Latif, M., and T. P. Barnett, 1994: Causes of decadal climate variability over the North Pacific and North America. *Science,* **266,** 634–637.

——, and ——, 1996: Decadal climate variability over the North Pacific and North America: Dynamics and predictability. *J. Climate,* **9,** 2407–2423.

Leblond, P. H., and L. A. Mysak, 1978: *Waves in the Ocean.* Elsevier, 602 pp.

Liu, Z., 1993: Interannual positive feedbacks in a simple extratropical air–sea coupling system. *J. Atmos. Sci.,* **50,** 3022–3028.

Marshall, J., and D. So, 1990: Thermal equilibration of planetary waves. *J. Atmos. Sci.,* **47,** 963–978.

Neelin, J., and W. Weng, 1999: Analytical prototypes for ocean–atmosphere interaction at midlatitudes. Part I: Coupled feedbacks as a sea surface temperature dependent stochastic process. *J. Climate,* **12,** 697–721.

Osychny, V., and P. Cornillon, 2004: Properties of Rossby waves in the North Atlantic estimated from satellite data. *J. Phys. Oceanogr.,* **34,** 61–76.

Pedlosky, J., 1987: *Geophysical Fluid Dynamics.* Springer-Verlag, 710 pp.

Pierce, D., T. P. Barnett, N. Schneider, R. Saravanan, D. Dommenget, and M. Latif, 2001: The role of ocean dynamics in producing decadal climate variability in the North Pacific. *Climate Dyn.,* **18,** 51–70.

Preisendorfer, R. W., and C. D. Mobley, 1988: *Principal Component Analysis in Meteorology and Oceanography.* Elsevier, 425 pp.

Qiu, B., W. Miao, and P. Müller, 1997: Propagation and decay of forced and free Rossby waves in off-equatorial oceans. *J. Phys. Oceanogr.,* **27,** 2405–2417.

Santoso, A., and M. H. England, 2004: Antarctic intermediate water circulation and variability in a coupled climate model. *J. Phys. Oceanogr.,* **34,** 2160–2179.

Shutts, G., 1987: Some comments on the concept of thermal forcing. *Quart. J. Roy. Meteor. Soc.,* **113,** 1387–1394.

van der Avoird, E., H. Dijkstra, J. Nauw, and C. Schuurmans, 2002: Nonlinearly induced low-frequency variability in a midlatitude coupled ocean-atmosphere model of intermediate complexity. *Climate Dyn.,* **19,** 303–320.

von Storch, H., and A. Navarra, Eds., 1999: *Analysis of Climate Variability.* Springer-Verlag, 342 pp.

——, and F. W. Zwiers, 2001: *Statistical Analysis in Climate Research.* Cambridge University Press, 484 pp.

White, W. B., 2000a: Coupled Rossby waves in the Indian Ocean on interannual timescales. *J. Phys. Oceanogr.,* **30,** 2972–2988.

——, 2000b: Tropical coupled Rossby waves in the Pacific ocean–atmosphere system. *J. Phys. Oceanogr.,* **30,** 1245–1264.

——, 2001: Evidence for coupled Rossby waves in the annual cycle of the Indo-Pacific Ocean. *J. Phys. Oceanogr.,* **31,** 2944–2957.

——, 2004: Comments on "Synchronous variability in the Southern Hemisphere atmosphere, sea ice, and ocean resulting from the annual mode." *J. Climate,* **17,** 2249–2254.

——, and R. G. Peterson, 1996: An Antarctic circumpolar wave in surface pressure, wind, temperature and sea-ice extent. *Nature,* **380,** 699–702.

——, Y. Ghao, and C. K. Tai, 1998: Coupling of biennial oceanic Rossby waves with the overlying atmosphere in the Pacific basin. *J. Phys. Oceanogr.,* **28,** 1236–1251.

Wunsch, C., and X. Zang, 1999: The observed dispersion relationship for the North Pacific Rossby wave motions. *J. Phys. Oceanogr.,* **29,** 2183–2190.

Yang, H., Z. Liu, and Q. Zhang, 2004: Tropical ocean decadal variability and resonance of planetary wave basin modes. Part II: Numerical study. *J. Climate,* **17,** 1711–1721.